



Anything but Little: a Pictorial Review on Anatomy and Pathology of the Cerebellum

Sven Dekeyzer^{1,2} · Stephanie Vanden Bossche^{2,3} · Laurens De Cocker⁴

Received: 24 April 2023 / Accepted: 9 June 2023 / Published online: 6 July 2023
© The Author(s), under exclusive licence to Springer-Verlag GmbH Germany 2023

Abstract

Despite its small size the cerebellum is an anatomically complex and functionally important part of the brain. Traditionally the cerebellum is viewed as a motor control structure entirely devoted to motor control and learning, but recent functional magnetic resonance imaging (fMRI) studies demonstrated significant involvement of the cerebellum in higher order cognitive functions. The anatomical complexity of the cerebellum is reflected by the several nomenclature systems that exist for the description of cerebellar anatomy. The cerebellum can be affected by a variety of pathological processes, including congenital, infectious and inflammatory, neoplastic, vascular, degenerative and toxic metabolic diseases. The purpose of this pictorial review is to (1) provide a general overview of cerebellar anatomy and function, (2) demonstrate normal cerebellar anatomy on imaging studies, and (3) illustrate both common as well as rare pathological conditions affecting the cerebellum.

Keywords Cerebellar anatomy · Neuroanatomy · Cerebellar atrophy · Radiology · Cerebellar pathology

Anatomy and Function

Normal Cerebellar Anatomy

The cerebellum (Latin for little brain) is located at the base of the brain, with the cerebrum superior and the brainstem anterior to it. The cerebellum takes up only 10% of the total brain volume, but despite its small size contains 80% of the brain neurons [1]. The cerebellum is separated from the overlying cerebrum by the tentorium cerebelli, a layer of tough dura mater, and is connected to the brainstem (and through the brainstem to the rest of the CNS) by three pairs of cerebellar peduncles.

The cerebellum consists of gray matter, central white matter and deep gray nuclei. The gray matter is located on the surface of the cerebellum and is tightly folded into large lobules and small folia. The central white matter, also called the corpus medullare, branches out towards to cerebellar lobules and folia, a pattern sometimes referred to as the *arbor vitae* because of its tree-like appearance. Embedded within the cerebellar white matter there are four pairs of deep cerebellar nuclei which provide the sole neural output from the cerebellum to the rest of the brain and consist of, from lateral to medial the dentate nucleus, the nucleus emboliformis, the nucleus globosus and the nucleus fastigii.

Macroscopically the cerebellum contains two hemispheres and a narrow midline zone called the vermis. The cerebellar hemispheres and the vermis are typically divided into three anatomical lobes: the anterior lobe, the posterior lobe and the flocculonodular lobe, which are separated by the primary fissure and the posterolateral fissure, respectively. Additional fissures subdivide the cerebellar lobes into numerous lobules. Many nomenclature systems exist for the description of the normal lobular anatomy of the cerebellum [2, 3]. This paper illustrates cerebellar lobular anatomy with common names used in the classical nomenclature and with the numerical classification as introduced by Schmahmann et al. (Table 1, Fig. 1; [2–6]).

✉ Sven Dekeyzer
sven.dekeyzer@gmail.com

¹ Department of Radiology and Medical Imaging, Ghent University Hospital (UZG), Corneel Heymanslaan 10, 9000 Gent, Belgium

² Department of Radiology, Antwerp University Hospital (UZA), Drie Eikenstraat 655, 2650 Edegem, Belgium

³ Department of Radiology, AZ Sint Jan Bruges, Ruddershove 10, 8000 Bruges, Belgium

⁴ Department of Radiology, AZ Maria Middelares Gent, Buitenhof-Sint-Denijs 30, 9000 Gent, Belgium

Table 1 Nomenclature of the cerebellar lobules. Column 1 illustrates the numerical nomenclature introduced by Schmahmann et al. (1999) [2]. Columns 2 and 3 contain common names for the cerebellar vermis and hemispheres, respectively [3]

Numerical	Vermis	Hemispheres	Lobes
I, II	Lingula	Vinculum	<i>Anterior lobe</i>
III	Central lobule	Wing of central	
IV	Culmen	Anterior quadrangular	
V			
VI	Declive	Posterior quadrangular	<i>Posterior lobe</i>
VIIAf	Folium	Superior semilunar	
VIIAt	Tuber	Inferior semilunar	
VIIIB		Gracile	
VIIIA	Pyramis	Biventral	
VIIIB			
IX	Uvula	Tonsil	
X	Nodulus	Flocculus	<i>Flocculonodular lobe</i>

Recognition of the different cerebellar lobules can be quite difficult (to near impossible) in the axial plane due to radial organization of the cerebellar lobules, but several important landmarks, such as the primary and prepyramidal fissure in the vermis, and the posterosuperior and horizontal fissure in the cerebellar hemispheres, are easy to recognize in the sagittal and coronal planes and allow further discrimination of the different cerebellar lobules (Figs. 2, 3 and 4).

Each lobule or sublobule contains several small ridges or gyri, which are called folia (singular: folium). The folium can be considered the basic structural anatomical unit of the cerebellum and contains a small core of white matter surrounded by a thin mantle of cortex. The extremely folded

nature of the cerebellum, primarily in large lobules and secondarily in multiple small folia, explains why the cortical surface area of the cerebellum is almost 80% of that of the cerebrum [7].

Of the four cerebellar nuclei only the dentate nucleus can consistently be detected on routine 1.5T or 3T MR imaging and is best seen on T2-weighted images (Fig. 5). The dentate nucleus gets its name from its tooth-like or serrated lateral edge which consists of gray matter. The medial/central part of the dentate nucleus consists of white matter, is called the hilum, and contains most of the afferents that exit from the dentate nucleus to the superior cerebellar peduncle.

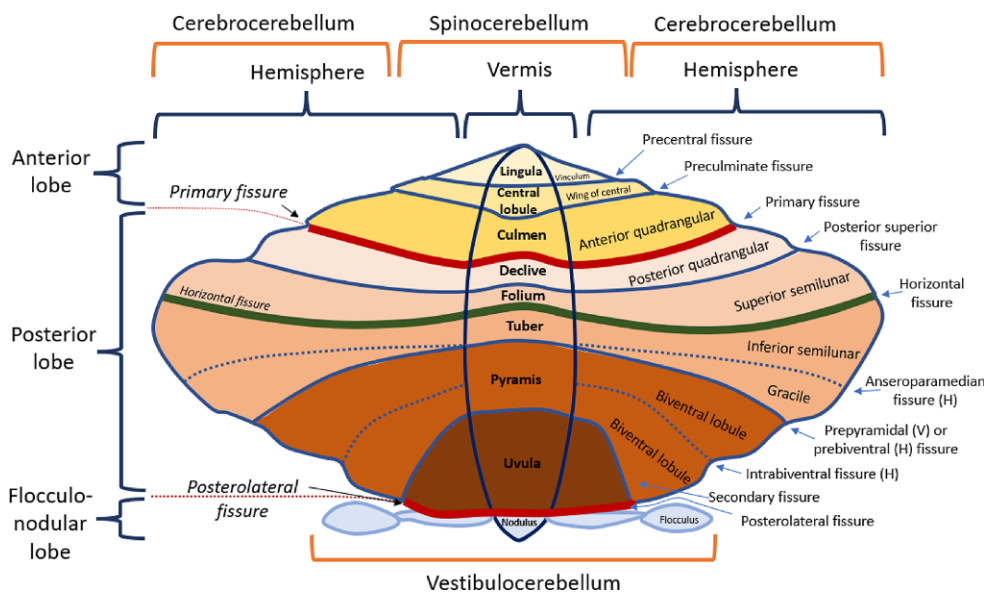


Fig. 1 Cerebellar anatomy as illustrated on the flattened cerebellar surface. Mediolaterally the cerebellum is composed of a central part (the vermis) and two lateral parts (the cerebellar hemispheres). Rostrocaudally, the cerebellum is typically divided into three lobes: the anterior lobe, posterior lobe, and flocculonodular lobe. Common names of cerebellar lobules and fissures are given. When a fissure is followed by (V) or (H) this refers to the name of this lobule or fissure in the vermis cerebelli (V) or cerebellar hemisphere (H), respectively. Functionally the cerebellum is classically divided into the spinocerebellum, cerebrocerebellum and vestibulocerebellum

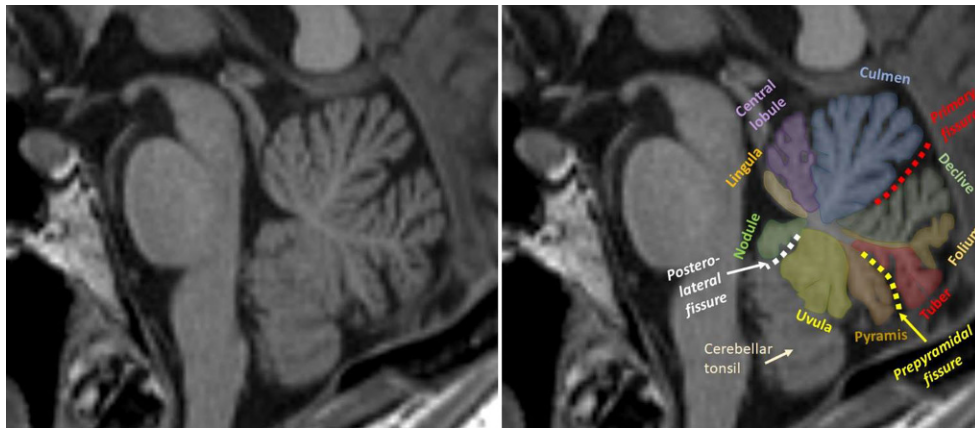


Fig. 2 The lobules and fissures of the vermis cerebelli illustrated on a midsagittal T1-weighted image. The most important (and easily recognizable) landmark in the vermis cerebelli is the primary fissure (red dotted line), which separates the anterior from the posterior lobe. The prepyramidal fissure (yellow dotted line) divides the posterior lobe in two easily identifiable parts, the upper/posterior part containing the declive, folium and tuber, and the inferior/anterior part containing the pyramis and uvula. The posterolateral fissure (white dotted line) is small and not always easy to delineate and separates the posterior lobe from the flocculonodular lobe. The cerebellar tonsil is part of the cerebellar hemispheres, not of the vermis, but can often be seen on midsagittal images due to partial volume averaging. The cerebellar tonsil is the hemispheric equivalent of the vermian uvula, while the flocculus is the equivalent of the nodule

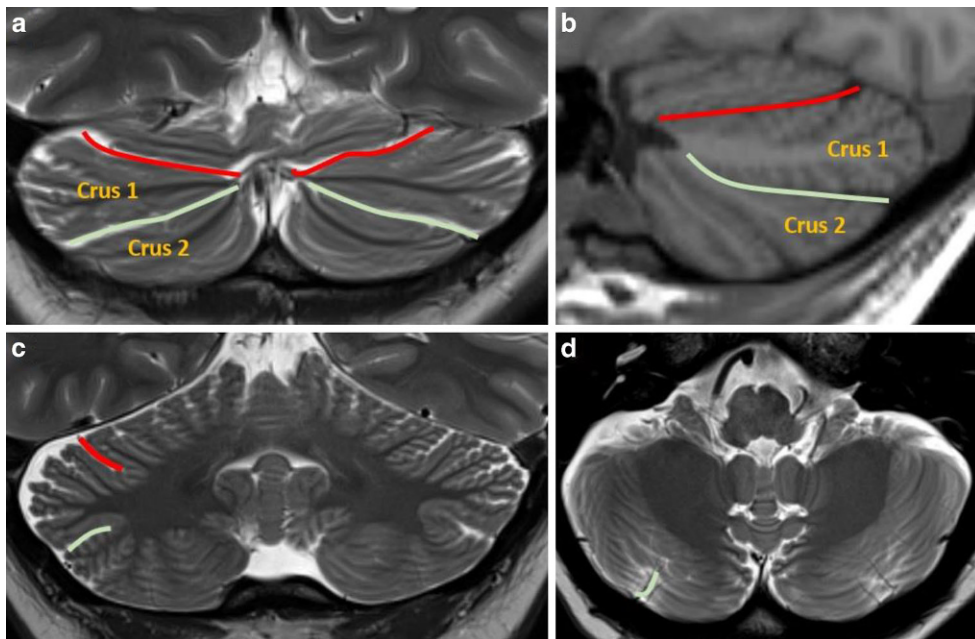


Fig. 3 Fissural landmarks in the cerebellar hemispheres. The posterior superior (red) and horizontal fissures (green) are important cerebellar hemispheric anatomic landmarks and can be easily identified in the coronal (**a**,**c**) and sagittal (**b**) planes. Posteriorly in the cerebellar hemispheres the posterosuperior (red) and horizontal fissure (green) converge and form an X-shape together with their contralateral homologues (**a**). By scrolling back to forth we recognize the posterosuperior and horizontal fissures in the cerebellar hemispheres more anteriorly in the coronal plane (**c**). In the sagittal plane (**b**), the posterosuperior (red) and horizontal fissure (green) converge anteriorly. In the axial plane (**d**), the horizontal fissure (green) can often be recognized as a small fissure running slightly perpendicular to the cerebellar cortex from inferolaterally to superomedially. Between the posterosuperior and horizontal fissure we find the superior semilunar lobule, also called Crus 1 (**a**, **b**). Under the horizontal fissure we find the inferior semilunar lobule, also called Crus 2 (**a**, **b**)

Three paired cerebellar peduncles connect the cerebellum to different parts of the nervous system. These are the superior cerebellar peduncles, the middle cerebellar peduncles, and the inferior cerebellar peduncles (Fig. 5). The superior cerebellar peduncle provides output to the cerebral

cortex and receives input from the ventral spinocerebellar tract. The middle cerebellar peduncle is connected to the pons and receives all its input from the pons, mainly from the pontine nuclei. The inferior cerebellar peduncle receives input from the vestibular nuclei, spinal cord and

Fig. 4 The flocculonodular lobe is designated with the Roman numeral X in the Schmahmann classification. In the vermis cerebelli we find the nodulus (X in **a**) which the flocculus is equivalent to in the cerebellar hemispheres (X in **b**). On these images we can also see the cerebellar tonsils (IX in **a**; IX and colored blue in **b**, **c**), the medial most inferior part of the cerebellar hemispheres and the cerebellar hemispheric equivalent of the uvula in the vermis. Also seen is the dentate nucleus (d.N. in **a** and **c**)

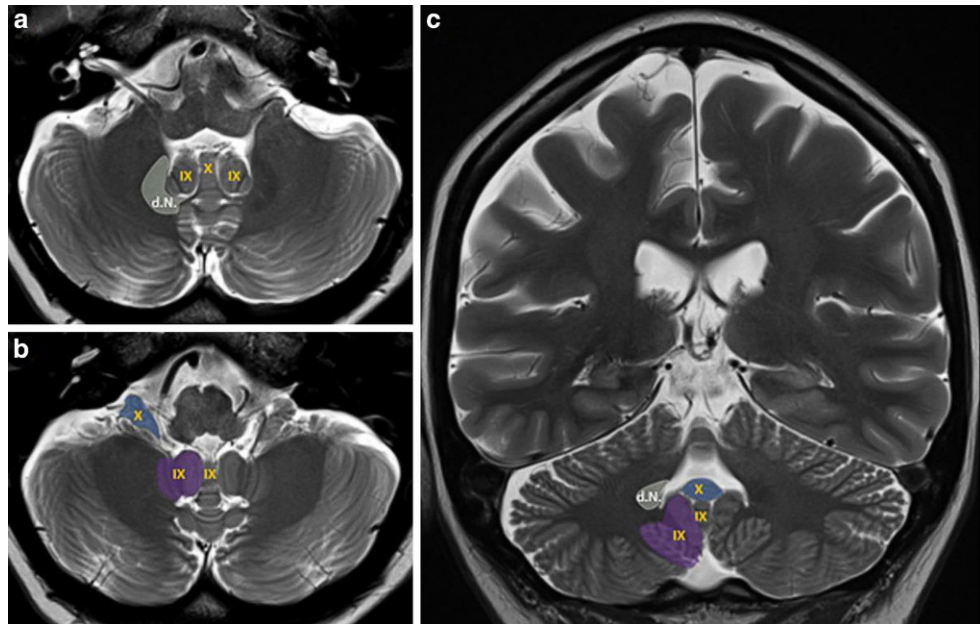
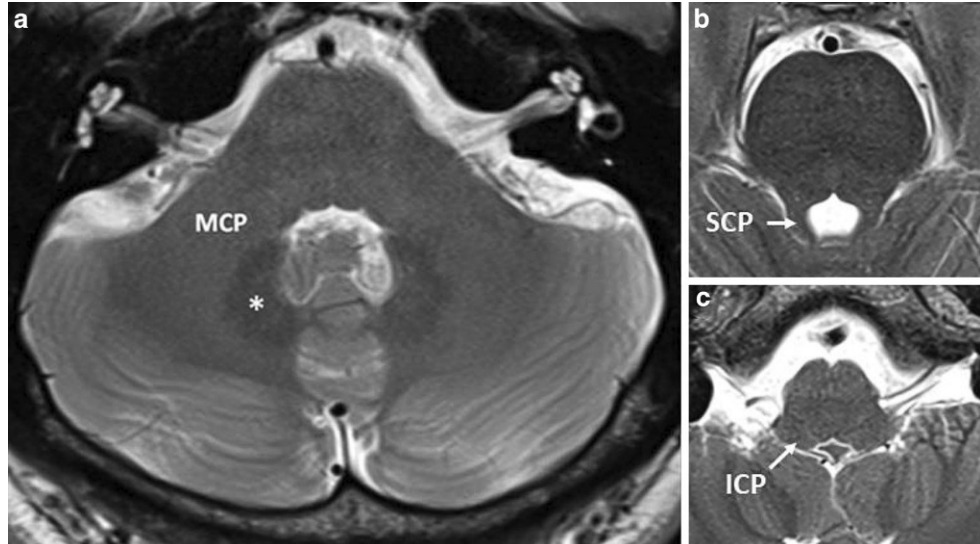


Fig. 5 The dentate nucleus and cerebellar peduncles. The dentate nucleus (asterisk in **a**) is best seen on T2-weighted images as it becomes slightly hypointense with increasing age. The lateral border of the dentate nucleus has a tooth-like serrated edge. Also shown are the cerebellar peduncles: the middle cerebellar peduncles at the level of the pons (MCP in **a**), the superior cerebellar peduncle at the level of the pontomesencephalic junction (SCP in **b**), and the inferior cerebellar peduncles at the level of the medulla oblongata (ICP in **c**)



the tegmentum and sends output to the vestibular nuclei and the reticular formation.

Arterial Supply of the Cerebellum

The cerebellum receives its arterial supply from three paired arteries that originate from the vertebrobasilar system: the superior cerebellar artery (SCA), the anterior inferior cerebellar artery (AICA) and the posterior inferior cerebellar artery (PICA). Usually, the PICA originates from the V4-segment of the vertebral artery, the AICA originates from the basilar artery, and the SCA branches off immediately underneath the junction point of the basilar artery and the posterior cerebral artery. Variant anatomy is common and

includes duplication, double origin and absence or dominance of a cerebellar artery, and occasionally a common PICA-AICA trunk may be observed [8]. The PICA supplies the posterior-inferior portion of the cerebellum [9]. The AICA supplies the anterior-inferior portion of the cerebellum. The extent of the AICA territory varies in reciprocity with the PICA and SCA territories. The SCA supplies the superior part of the cerebellum. The cerebellar arteries also vascularize the lateral and posterior brainstem, so occlusions of these arteries can give rise to various brainstem syndromes in combination with cerebellar symptoms. The best-known example is a PICA infarction that involves the posterolateral medulla oblongata and typically manifests as Wallenberg's syndrome.

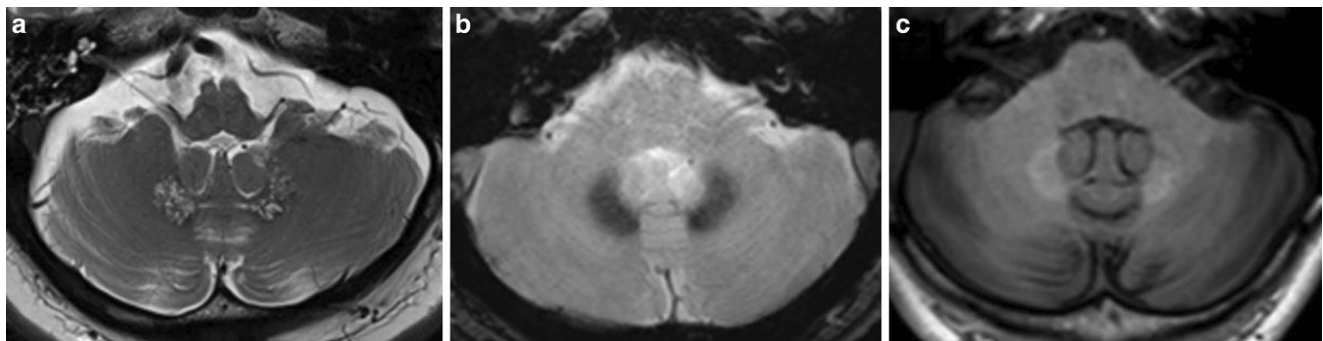


Fig. 6 Frequent variants in the dentate nucleus. Axial TSE T2-weighted images (a) show multiple slightly enlarged Virchow-Robin spaces in a patient who also had diffuse widening of perivascular spaces in the basal ganglia (so-called *état criblé*). Axial GRE T2*-weighted images in a different patient (b) show signal decrease in the dentate nuclei. This is often seen in older patients in conjunction with T2*-signal decrease in the basal ganglia and is caused by age-related iron deposition. Axial GRE T1-weighted images (c) in a patient with multiple sclerosis who received repeated MRI with gadolinium in the past show spontaneously T1-hyperintense dentate nuclei due to gadolinium deposition

Cerebellar Function

The cerebellum plays an important role in motor control and motor learning. Functionally, the cerebellum can be divided into three zones that do not correspond to the anatomical subdivisions of the cerebellum: the vestibulocerebellum, the spinocerebellum and the cerebrocerebellum (Fig. 1).

The vestibulocerebellum is phylogenetically the oldest part of the cerebellum and corresponds to the flocculonodular lobe. The vestibulocerebellum receives input from the vestibular system and its main function is to control equilibrium and eye movements.

The spinocerebellum comprises the vermis and the paravermis (the paravermis being the medial most part of the cerebellar hemispheres). The spinocerebellum receives direct input from the spinal cord and facilitates smooth muscle movements and motion error correction.

Lastly, the cerebrocerebellum, phylogenetically the most recent part of the cerebellum, receives its input from many different areas of the cerebral cortex and interacts with the motor cortex to plan and program movements.

More recently, functional magnetic resonance imaging (fMRI) studies have found that the majority of the cerebellum is dedicated to non-motor functions [10]. In the cerebellar topographic organization, cognitive functions seem to be localized laterally and sensorimotor functions medially.

Imaging of Cerebellar Pathology

Incidental Findings

Occasionally, small Virchow-Robin spaces can be seen in the dentate nuclei (Fig. 6). Age-related iron deposition, a finding commonly seen in the basal ganglia of older patients as areas of low signal intensity on gradient echo (GRE) T2*-images or susceptibility weighted

images (SWI), can also be present in the dentate nuclei (Fig. 6; [11]). Contrary to what is observed in the basal ganglia, physiological age-related calcifications are infrequently found in the dentate nuclei. Increased T1-signal can be observed in the dentate nucleus of patients who have undergone repeated contrast enhanced MRI and reflects gadolinium deposition. The significance of this last finding is still unclear (Fig. 6; [12]).

Vascular Disorders

Acute Ischemic Stroke

Cerebellar infarcts account for ~2% of acute ischemic strokes [13], although this number might be much higher as most cerebellar infarcts are small and may initially remain unnoticed.

Large cerebellar infarcts affect the PICA territory much more frequently than the AICA or SCA territories. Initial symptoms of large cerebellar infarction may be nonspecific, such as headache, dizziness, nausea, vomiting and vertigo. More than half of patients with cerebellar stroke present with nausea and vomiting, and about 75% present with dizziness [13]. Therefore, cerebellar infarction must be considered when patients present with acute nonspecific symptoms. As in supratentorial ischemic stroke unenhanced CT may show obscuration of gray-white matter differentiation, and MRI shows a T2-hyperintense region of pathological diffusion restriction on diffusion-weighted imaging (DWI) corresponding to the vascular territory involved (Fig. 7).

Small cerebellar infarcts often remain unnoticed and are hence rarely detected in the acute stage. They are often seen as incidental findings on imaging studies in older patients and typically manifest as small (generally <2 cm), linear (needle-like) or wedge-shaped cavities in the posteroinferior part of the cerebellar hemispheres (Fig. 8; [14]). They show a remarkable affinity for the cerebellar cortex with

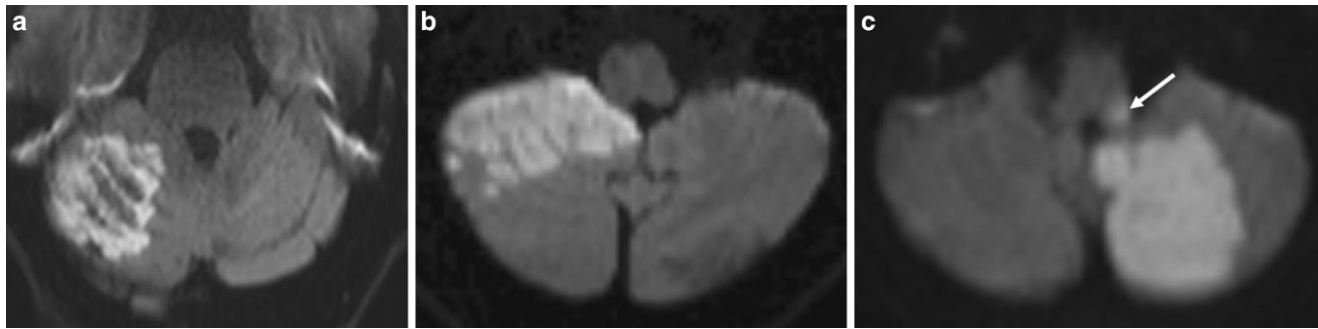


Fig. 7 Acute large cerebellar infarcts due to large vessel occlusions. Diffusion-weighted images show diffusion restrictive areas in the cerebellar hemispheres corresponding to the vascular territories of the superior cerebellar artery (a), the anterior inferior cerebellar artery (b) and the posterior inferior cerebellar artery (c). SCA infarcts involve the superior surface of the cerebellum (a). AICA and PICA infarcts involve the inferior part of the cerebellum, with the AICA territory situated anteriorly (b) and the PICA territory posteriorly (c). Notice that PICA infarct may also involve the ipsilateral posterolateral part of the medulla oblongata (arrow in c) giving rise to Wallenberg syndrome

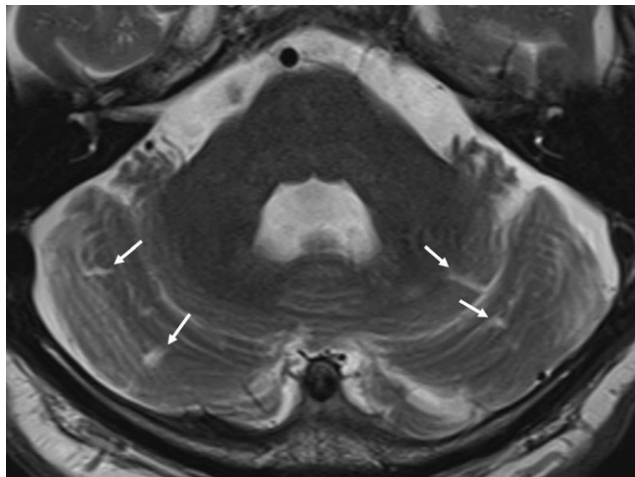


Fig. 8 Sequela of small cerebellar infarct as an incidental finding on T2-weighted MRI images in an older patient. Several small punctate and linear cerebrospinal fluid (CSF)-filled tissue defects (arrows) are seen in the cortical gray matter of the posterior cerebellum. These infarcts are known as cerebellar cortical infarct cavities and also as cerebellar needle infarcts

sparing of subjacent white matter, and often occur in the apex of cerebellar fissures, hence the apex sign or depth of fissure sign [14–16]. They are believed to be the result of thromboembolic stroke with occlusion of small cerebellar end arteries, and they may also be seen in watershed infarctions due to decreased wash-out of emboli [17–19].

Cerebellar Hemorrhage

Cerebellar hemorrhages account for approximately 10% of all intracranial hemorrhages [20].

Primary hypertensive hemorrhage is the most frequent type of cerebellar hemorrhage and is most frequently seen in middle-aged and older patients with longstanding poorly controlled hypertension. Hypertensive cerebellar hemorrhages are typically located deep/centrally in the cerebellar hemispheres at the dentate nuclei. Other stigmata of chronic

hypertensive encephalopathy are usually present on CT or MRI (Fig. 9).

Other possible causes include vascular malformations, hemorrhagic tumors and cerebral amyloid angiopathy (CAA). Cerebellar hemorrhages in CAA tend to be more superficially located at the cerebellar cortex (Fig. 9; [21]). CT-angiography or MRI abnormalities that are suggestive of dural arteriovenous fistula (dAVF) are the presence of prominent engorged cerebellar veins and abnormal early enhancement of dural sinuses (Fig. 9; [22]).

A Special Form of Cerebellar Hemorrhage is the Remote Cerebellar Hemorrhage A remote cerebellar hemorrhage is a complication of supratentorial craniotomy, spinal surgery, lumbar puncture or insertion of a lumboperitoneal shunt. Patients are generally asymptomatic and the hemorrhage is benign in most cases. On imaging layering of subarachnoid blood in the superior cerebellar fissures can be seen (sometimes referred to as the zebra sign) (Fig. 10). The pathophysiology of this entity remains unknown. One theory is that intracranial hypotension due to cerebrospinal fluid (CSF) loss causes cerebellar sagging and occlusion of superior perforating cerebellar veins leading to hemorrhagic infarction [23].

Infectious and Inflammatory Disorders

Bacterial Infections

Pyogenic cerebellar abscesses are secondary to otomastoiditis in most cases [24]. They develop either from direct extension of a suppurative middle ear infection or mastoiditis, or through retrograde suppurative thrombophlebitis [24]. They are typically located in one cerebellar hemisphere and are often associated with ipsilateral transverse sigmoid sinus thrombosis. On MRI pyogenic abscesses present as mass lesions with a T2-hypointense, strongly enhancing

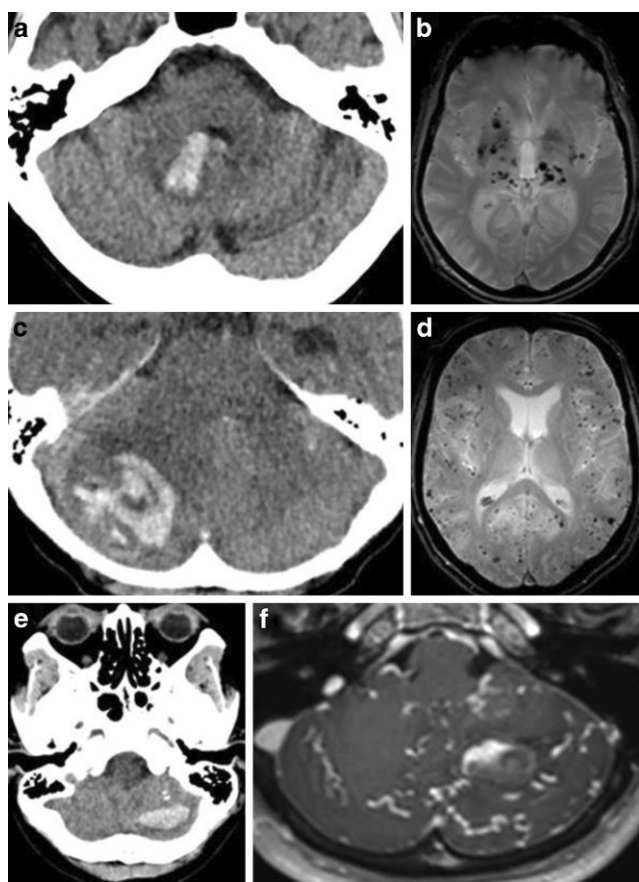


Fig. 9 Cerebellar hemorrhages in chronic hypertensive encephalopathy (**a, b**), cerebral amyloid angiopathy (**c, d**) and dural arteriovenous fistula (**e, f**). Primary hypertensive hemorrhage (**a, b**): Axial unenhanced CT shows a deep hemorrhage originating from the right dentate nucleus with extension into the 4th ventricle (**a**). Axial GRE T2*-image shows multiple microbleeds in the basal ganglia and thalamus, a pattern often seen in chronic hypertensive patients (**b**). Cerebral amyloid angiopathy (CAA)-related cerebellar hemorrhage (**c, d**): Axial unenhanced CT shows a peripherally located heterogeneous right cerebellar hemorrhage, which seems to originate from the cerebellar cortex rather than the deep white matter (**c**). Axial GRE T2*-images show dozens of peripherally located microbleeds with sparing of the basal ganglia, a pattern compatible with CAA (**d**). Cerebellar hemorrhage in dural arteriovenous fistula (**e, f**): Axial unenhanced CT shows a superficial intraparenchymal hemorrhage in the left cerebellar hemisphere (**e**). Two calcifications are seen anterior to the hemorrhage. On axial T1-weighted images with gadolinium (**f**) multiple engorged cerebellar veins are seen in both cerebellar hemispheres, which is suggestive for a dural arteriovenous fistula with venous cortical reflux. This was later confirmed by digital subtraction angiography (DSA)

capsule surrounding a nonenhancing necrotic T2-hyperintense center filled with diffusion restrictive pus (Fig. 11). Dual-rim sign can be observed on SWI. The abscess stage is preceded by a cerebritis phase characterized by an ill-defined T2-hyperintense zone of inflammation, often with diffusion restriction and some patchy enhancement, but no recognizable capsule.

Listeria rhombencephalitis is an infection of the brain-stem and/or cerebellum (the rhombencephalon) by *Listeria*

monocytogenes. *Listeria monocytogenes* is a Gram-positive bacterium that can cause meningitis, meningoencephalitis, or brain abscesses. Rhombencephalitis is a particular form of encephalitis that primarily affects the brain stem and cerebellum, and *Listeria* is reported as the most common etiology for rhombencephalitis [25]. Older and immunocompromised patients are at increased risk for *Listeria* central nervous system (CNS) infections; however, in contrast to other *Listeria* CNS infections *Listeria* rhombencephalitis is most frequently seen in immunocompetent young adults [26]. *Listeria* rhombencephalitis is often misdiagnosed initially because prodromal symptoms are nonspecific and meningeal signs are uncommon; however, early initiation of antibiotic treatment is crucial for survival and the reduction of neurologic sequelae. The imaging characteristics are dependent on the stage in which the infection is detected and imaging findings compatible with cerebritis and abscess can be seen, with a predilection for the dorsal brainstem and cerebellum, especially the floor of the 4th ventricle (Fig. 12).

Parainfectious and Postinfectious Cerebellitis

Acute cerebellitis and acute cerebellar ataxia (or acute postinfectious cerebellar ataxia) are terms that are often used interchangeably and probably represent different spectra of the same disease process. Acute cerebellitis and acute cerebellar ataxia refer to the acute onset of cerebellar symptoms, usually in children and probably resulting from parainfectious or postinfectious cerebellar immune-mediated inflammation. Evidence of direct CNS infection is rarely found. Infectious diseases associated with acute cerebellitis include Epstein-Barr virus, influenza A and B, mumps, varicella zoster virus, coxsackie virus, rotavirus, echovirus and *Mycoplasma* pneumonia. A preceding varicella zoster infection is the most frequently reported association. Rare cases of postvaccination cerebellitis have also been reported [24].

The term acute cerebellar ataxia is generally reserved for milder cases characterized by an acute onset of cerebellar symptoms without signs of increased intracranial pressure, with normal neuroimaging studies, and a benign self-limiting disease course. The term acute cerebellitis is used for more severe cases, in which cerebellar symptoms are often overshadowed by altered consciousness and signs of increased intracranial pressure caused by cerebellar swelling and/or hydrocephalus. These patients often have abnormal neuroimaging studies and a worse disease course and prognosis. The use of MRI can show unilateral or bilateral cerebellar swelling, with T2-hyperintensity of the cerebellar cortex and/or subcortical or deep white matter (Fig. 13). Leptomeningeal contrast enhancement can be seen in the cerebellar fissures. In the acute stage pathological diffu-

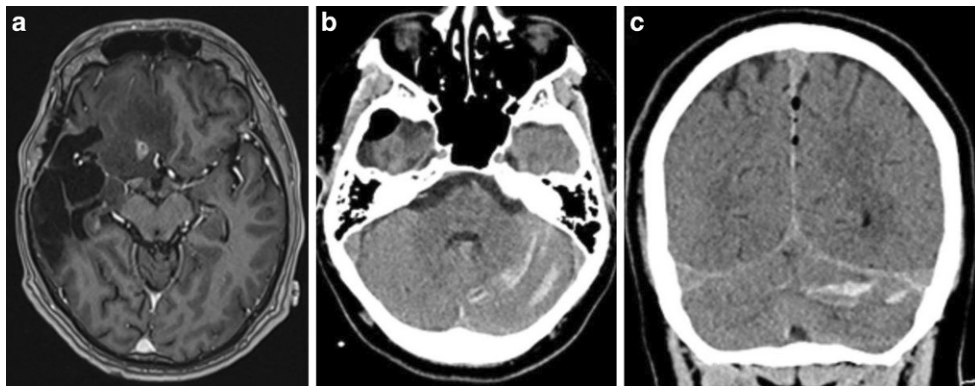


Fig. 10 Remote cerebellar hemorrhage: patient with a recurring high-grade glial tumor in the right frontal lobe (after right temporal tumorectomy) on axial T1-weighed images after gadolinium (**a**). Partial tumor resection was performed. On postoperative unenhanced CT a subarachnoid hemorrhage is seen along the left cerebellar hemisphere, extending in multiple cerebellar fissures and resulting in the so-called zebra-sign (**b, c**). (case courtesy of dr. Sofie Van Cauter, Ziekenhuis Oost-Limburg (ZOL) Genk, Belgium)

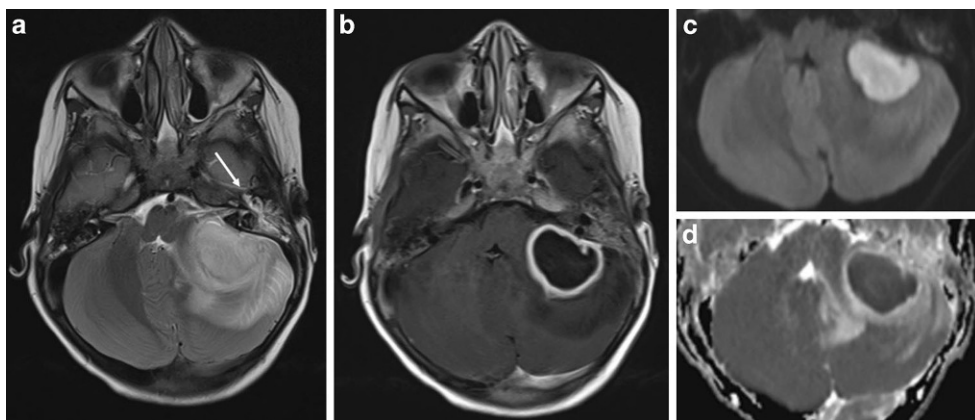


Fig. 11 Pyogenic cerebellar abscess in an 11-year-old girl. Axial T2-weighted images show an intra-axial T2-hyperintense mass lesion with a T2-hypointense rim and extensive perilesional edema in the left cerebellar hemisphere (**a**). Notice fluid-filled left-sided mastoid air cells with mucosal contrast enhancement (**b**), suggestive of an ipsilateral otomastoiditis (arrow in **a**). The lesion has a thick enhancing capsule on post-contrast T1-weighted images (**b**) and the non-enhancing center of the lesion has a high signal on diffusion-weighted images (**c**) and a low signal on the ADC-map (**d**), reflecting true diffusion restriction in pus

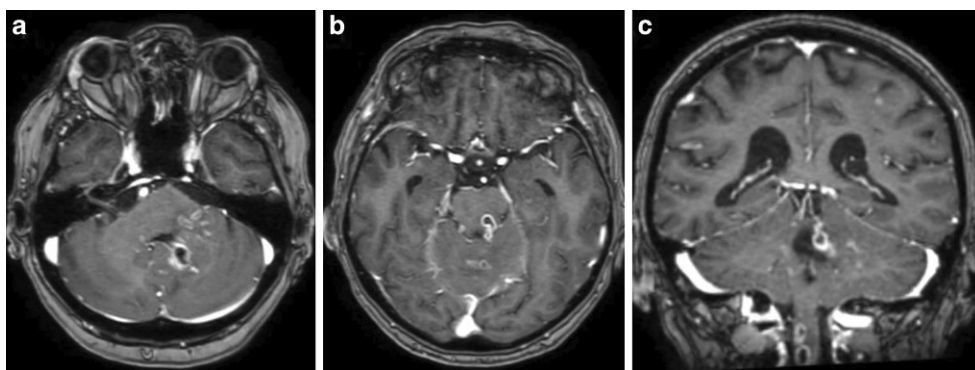


Fig. 12 *Listeria* rhombencephalitis in an older patient. Axial (**a, b**) and coronal (**c**) reconstructions of a 3D-T1 sequence with gadolinium shows multiple irregular rim-enhancing lesions of variable sizes in the brainstem (**a**), left middle cerebellar peduncle and cerebellum around the posterior border of the 4th ventricle (**b**) and also the upper cervical spinal cord (**c**). (case courtesy of dr. Sofie Van Cauter, Ziekenhuis Oost-Limburg (ZOL) Genk, Belgium)

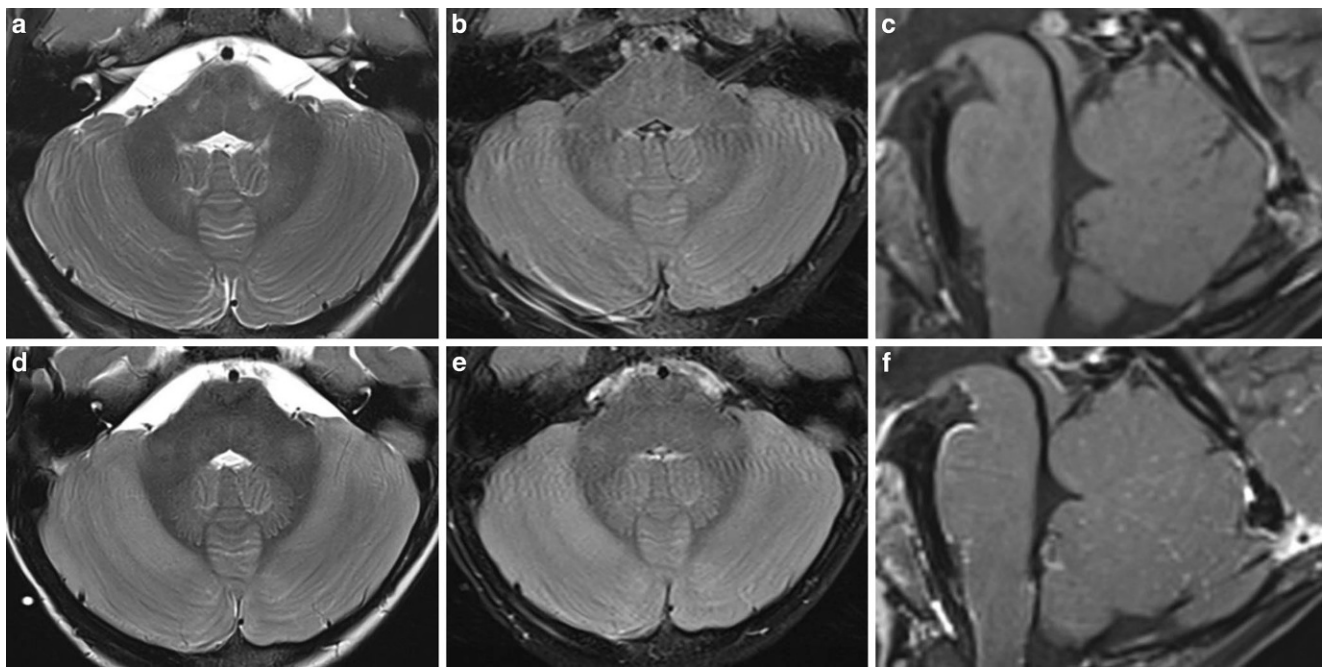


Fig. 13 Acute cerebellitis in a young girl presenting with acute cerebellar ataxia. MRI performed on day 1 (a–c) shows no abnormalities. Due to clinical deterioration a second MRI was performed a couple of days later (d–f). This time clear T2-hyperintense edematous changes are seen in the cerebellar cortex on T2-weighted (d) and FLAIR images (e). On contrast-enhanced TSE T1-weighted black blood images clear volume increase of the cerebellum is seen with obliteration of the cerebellar fissures as well as new patchy leptomeningeal enhancement (f)

sion restriction may be present. The cerebellar swelling can result in tonsillar herniation or obstructive hydrocephalus. On follow-up studies imaging abnormalities may disappear completely, or progress to cerebellar atrophy [24].

Paraneoplastic and Nonparaneoplastic Autoimmune Encephalitis

A paraneoplastic syndrome rather than an infection or postinfectious syndrome should be considered in adults with subacute cerebellar ataxia, especially in middle-aged and older patients. Paraneoplastic cerebellar degeneration is one of the most common paraneoplastic syndromes. Paraneoplastic cerebellar degeneration is an inflammatory autoimmune disorder that results from the destruction of cerebellar Purkinje cells by onconeural antibodies. These onconeural antibodies are produced by the immune system in response to a protein that is expressed by tumor cells. Multiple onconeural antibodies have been detected in patients with paraneoplastic cerebellar degeneration. Anti-Yo antibody, also known as anti-Purkinje cell cytoplasmatic antibody 1, is most commonly detected and is usually associated with breast and gynecological malignancies [27]. MRI may be normal or can show early T2-hyperintense edematous changes in the cerebellar cortex (Fig. 14), while cerebellar atrophy can be seen in end-stage disease (Fig. 15). Paraneoplastic cerebellar degeneration can be associated with meningeal contrast enhancement and ac-

cordingly falsely diagnosed as leptomeningeal cerebellar carcinomatosis [28].

Anti-GAD65 autoimmune encephalitis is a nonparaneoplastic autoimmune encephalitis typically occurring in young females. Three clinical syndromes have been described with anti-GAD65 encephalitis: refractory temporal lobe epilepsy, stiff-man syndrome, and cerebellar ataxia.

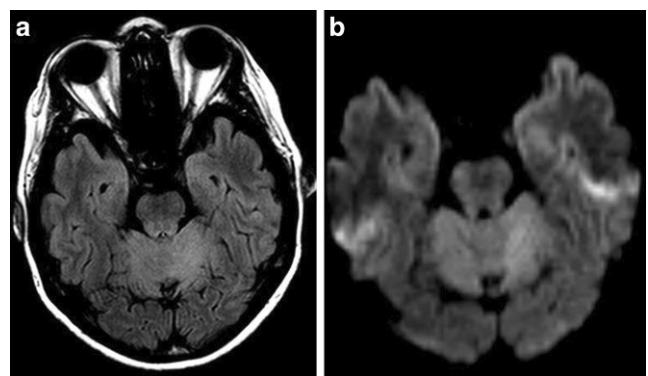


Fig. 14 Paraneoplastic cerebellar degeneration in a 53-year-old woman with breast cancer and anti-Yo antibodies who presented with subacute cerebellar ataxia. MRI in the subacute phase shows symmetrical hyperintense changes in the cerebellar hemispheres on FLAIR (a) and diffusion-weighted images (b). The images are strongly windowed to increase the contrast between the edematous cerebellar changes and the normal supratentorial structures. On follow-up positron emission tomography CT (PET-CT) performed 2 years later the patient had developed a significant cerebellar atrophy (images not shown)

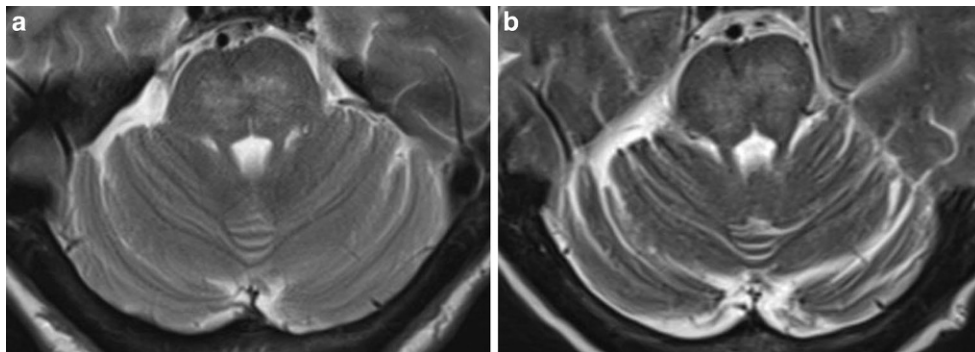
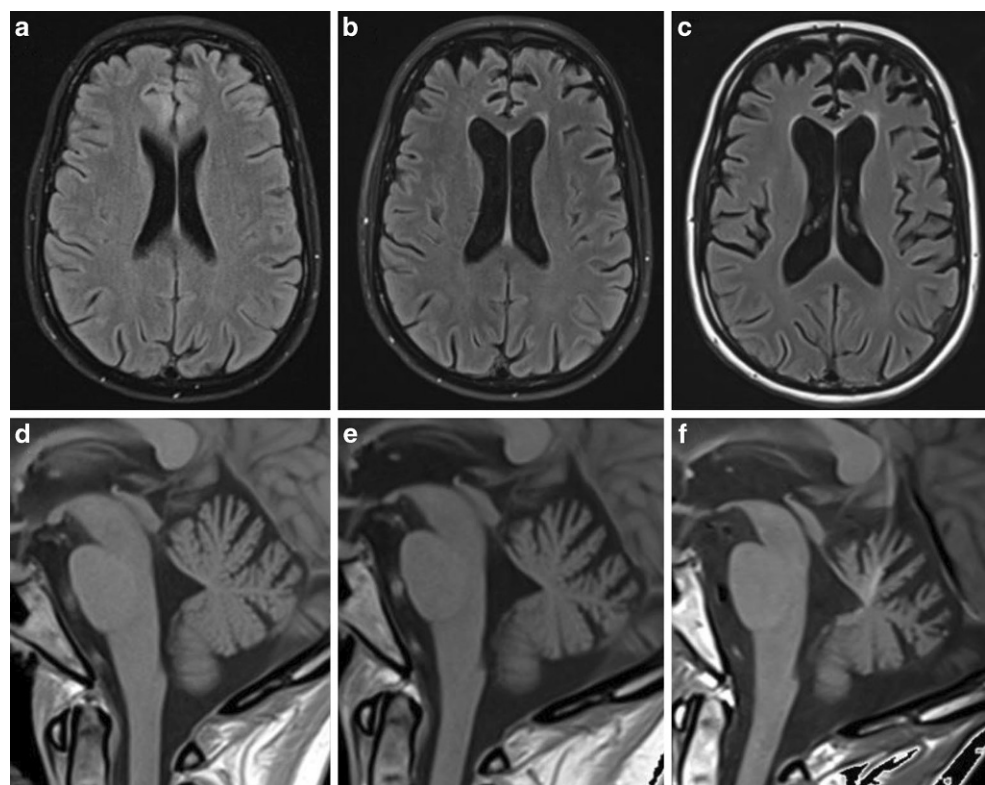


Fig. 15 Paraneoplastic cerebellar degeneration in a 69-year-old woman with a subacute cerebellar syndrome. On axial T2-weighted images of the MRI performed in the subacute phase (**a**) the cerebellum appears normal. Several months later the patient had developed a clear cerebellar atrophy with marked widening of the cerebellar fissures (**b**). Anti-Yo antibodies were detected in the CSF. The patient received whole body screening in which two breast cancers were detected

Fig. 16 Rapidly progressive cerebral and cerebellar atrophy in a 40-year-old woman with refractory epilepsy and anti-GAD65 autoimmune encephalitis. Images performed shortly after symptom onset (**a, d**), 2 months later (**b, e**) and 1 year later (**c, f**) show hyperintense changes of the right cingulate gyrus in the acute phase (**a**) with ensuing cerebral atrophy on axial FLAIR images (**a–c**) in combination with rapidly progressive cerebellar atrophy on magnified sagittal T1-weighted images (**d–f**)



On imaging age-disproportionate cerebral and cerebellar atrophy (either combined or in isolation) is observed in more than half of patients (Fig. 16; [29]).

CLIPPERS

CLIPPERS stands for chronic lymphocytic inflammation with pontine perivascular enhancement responsive to steroids. It is an uncommon and still poorly understood inflammatory CNS disorder with a unique imaging appearance characterized by multiple punctate and curvilinear perivascular foci of contrast enhancement “peppering the

pons” and adjacent rhombencephalic structures, such as the cerebellar peduncles, cerebellar hemispheres, medulla oblongata and midbrain (Fig. 17; [30]). The range of age at presentation is wide (13–86 years) and patients present with a variety of symptoms dominated by cranial nerve dysfunction, cerebellar symptoms and long tract symptoms. Patients typically respond rapidly to steroids but have a tendency to relapse after steroid treatment is stopped, so long-term immunosuppressive therapy is mandatory. When CLIPPERS is observed it is crucial to test for mimickers, such as myelin oligodendrocyte glycoprotein-associated disease (MOG-AD) [31].

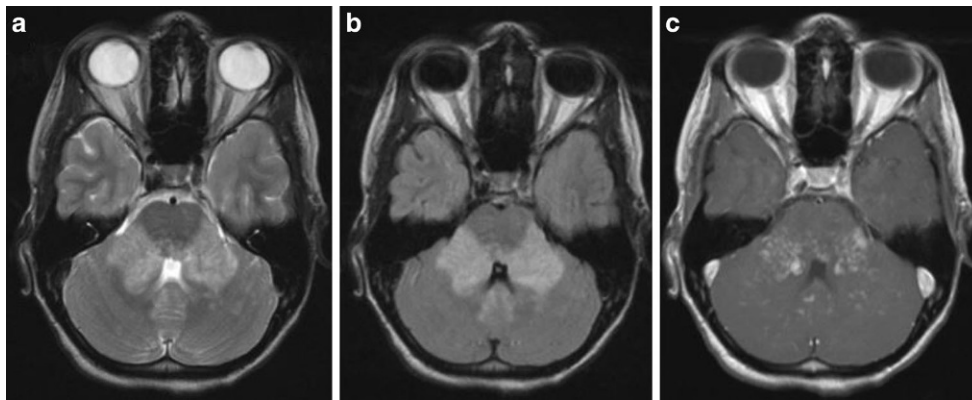


Fig. 17 CLIPPERS in a 17-year-old girl presenting with rapidly developing cerebellar and pyramidal symptoms. MRI of the brain shows hyperintense changes in both middle cerebellar peduncles and anteriorly in the vermis on T2-weighted (a) and FLAIR images (b). On axial T1-images with gadolinium multiple punctate and curvilinear foci of contrast enhancement are seen in the pons and cerebellum and are most extensive in both middle cerebellar peduncles (c). The clinical symptoms as well as the radiological abnormalities disappeared quickly following corticosteroid treatment

Progressive Multifocal Leukoencephalopathy

Progressive multifocal leukoencephalopathy (PML) is a demyelinating disorder resulting from reactivation of the John Cunningham virus (JC-virus) in the brains of immunosuppressed patients, mostly human immunodeficiency virus (HIV) patients or patients receiving immunosuppressant drugs that alter T-cell function. The JC-virus causes a lytic infection of oligodendrocytes and on MRI generally multifocal T2-hyperintense white matter lesions with little or no mass effect are seen, typically starting in the juxtacortical white matter. Contrast enhancement is usually absent, except in the context of PML immune reconstitution syndrome, and diffusion restriction may be seen at the leading edge of the lesion.

Posterior fossa involvement is frequently seen in PML [32]. Posterior fossa lesions typically affect the middle cerebellar peduncles and adjacent pons and/or cerebellar hemispheres. The “shrimp sign” is a radiological sign with a reported high specificity and sensitivity for the detection of fossa posterior PML. The shrimp sign refers to a T2 and FLAIR hyperintense, T1 hypointense lesions located in the

middle cerebellar peduncle with extension in the deep cerebellar white matter and abutment of the dentate nucleus (Fig. 18; [33]).

JC virus granule cell neuropathy is a rare manifestation of CNS infections by the JC virus in which the lytic infection predominantly occurs in the granule cell neurons of the cerebellum, leading to neuronal loss, gliosis, and cerebellar atrophy. JC virus granule cell neuropathy is less frequent than PML and most cases have been described in HIV-infected patients. Due to the rarity of the disease, imaging characteristics are not well described. The most characteristic imaging finding is cerebellar atrophy, which often occurs in combination with white matter changes in the cerebellum and brainstem [34].

Toxic-Metabolic Disease

Alcohol-Related Cerebellar Degeneration

The cerebellum, and particularly the Purkinje cells, are susceptible to many toxic agents, of which alcohol is the most common. Alcoholic cerebellar degeneration is related to ei-

Fig. 18 Shrimp sign in posterior fossa PML. A 56-year-old HIV-positive patient suffered an epileptic seizure. Axial FLAIR (a) and T2-weighted (b) MRI show a T2-hyperintense lesion without mass-effect extending from the left middle cerebellar peduncle into the deep white matter of the left cerebellar hemisphere, abutting but sparing the left dentate nucleus. PCR on spinal fluid was positive for JC virus

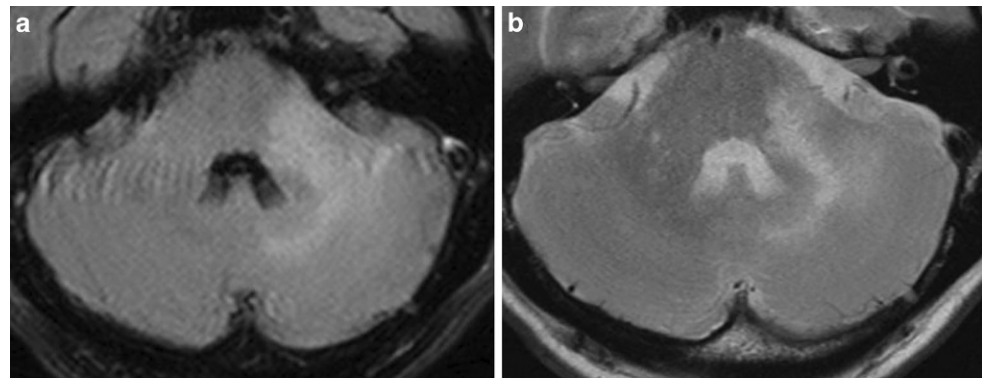
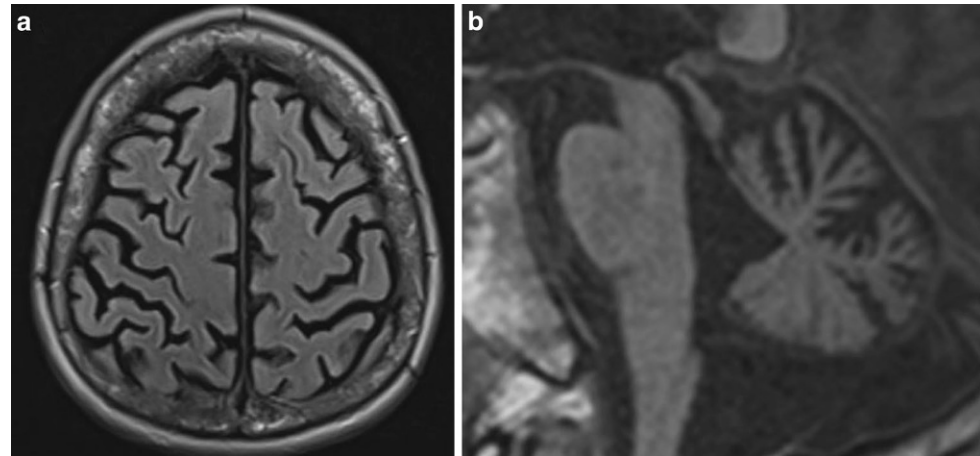


Fig. 19 Alcoholic cerebellar degeneration in a 48-year-old man with a chronic history of alcohol abuse. Axial FLAIR images (**a**) of the supratentorial brain structures show global cerebral atrophy (GCA 2) abnormal for age. Sagittal T1-weighted images (**b**) show pronounced vermian atrophy of both the anterior and posterior lobes



ther a direct toxic effect of alcohol on the Purkinje cells, nutritional deficiencies (especially of vitamin B1) or both [35]. Brain imaging in alcoholic cerebellar degeneration usually shows pronounced cerebellar atrophy that is abnormal for the patient's age, is typically most pronounced in the anterior vermis, and may be accompanied by generalized cerebral atrophy (Fig. 19).

Other Cerebellotoxic Agents

Metronidazole is an antibiotic used to treat a variety of bacterial and protozoan infections and can in rare instances lead to CNS toxicity. CNS toxicity usually occurs after several weeks of metronidazole treatment and patients present with signs of cerebellar dysfunction. Less frequent symptoms are altered mental state and seizures. On imaging nearly all patients show lesions in the cerebellum, particularly in both dentate nuclei (Fig. 20; [36]). Less frequently lesions are also observed in the splenium of the corpus callosum or the dorsal brainstem. Lesions are T2-hyperintense, nonenhancing and may show both increased and decreased diffusivity

on DWI. Imaging abnormalities resolve completely after discontinuation of the drug, and symptoms usually improve considerably or disappear completely [36].

Isoniazid is a tuberculostatic agent that can cause a dose-independent neurotoxic syndrome with clinical and imaging findings similar to metronidazole-induced neurotoxicity (Fig. 21; [36]).

Various anti-epileptic drugs are associated with cerebellar acute or chronic cerebellar toxicity. Chronic treatment with phenytoin and valproic acid is associated with drug-induced cerebellar atrophy (Fig. 22; [37]).

In heroin-induced leukoencephalopathy, a toxic leukoencephalopathy caused by the inhalation of heroin fumes (chasing the dragon), widespread involvement of supratentorial and infratentorial white matter can be seen. Infratentorially, extensive T2-hyperintense changes of the central white matter and middle cerebellar peduncles are often seen with either increased and decreased diffusivity on DWI (Fig. 23; [36]).

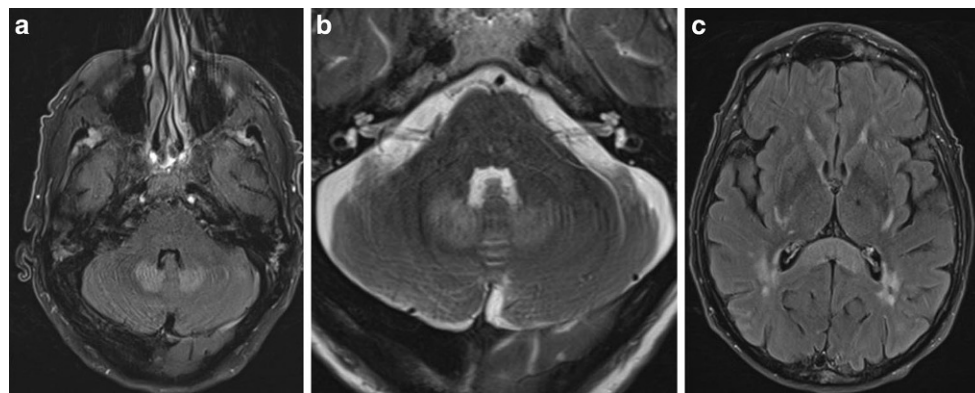


Fig. 20 Metronidazole-induced neurotoxicity in a 71-year-old man, under antibiotic treatment with metronidazole for a peridiverticular abscess, presenting with postural instability and gait ataxia. Axial FLAIR (**a**) and T2-weighted images (**b**) show symmetrical T2-hyperintense lesions in both dentate nuclei. Axial FLAIR images also show T2-hyperintensity in the splenium of the corpus callosum (**c**). There was no diffusion restriction or contrast enhancement (images not shown)

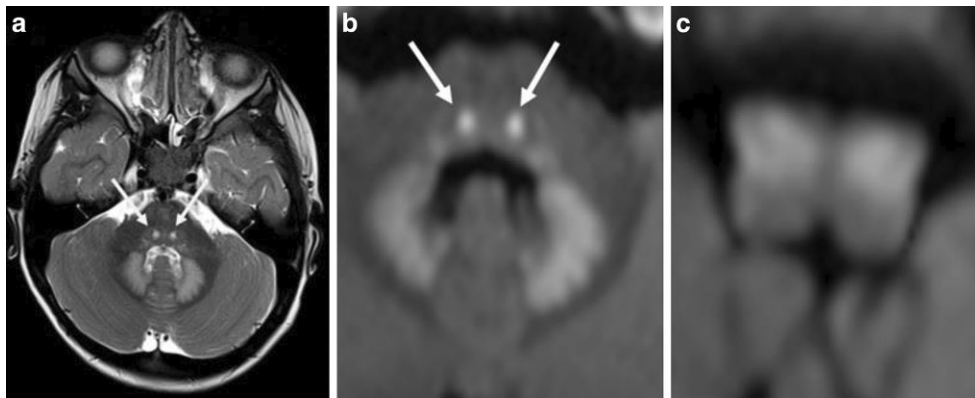


Fig. 21 Isoniazid-induced neurotoxicity in a 3-year-old boy under tuberculostatic treatment for tuberculous lymphadenitis. Axial T2-weighted images (a) show T2-hyperintensity in both dentate nuclei and bilateral central tegmental tracts (*arrows* in a and b). These abnormalities are clearly depicted and hyperintense on the magnified b1000-diffusion weighted images (b). The inferior olfactory nuclei in the medulla oblongata are hyperintense on diffusion weighted images (c) as well as the red nuclei (images not shown), so abnormalities were present in all components of the Guillain-Mollaret triangle

Fig. 22 Phenytoin-induced cerebellar atrophy in a patient with left-sided hippocampal sclerosis. Coronal T2-weighted images at the level of the hippocampi (a) shows evident left-sided mesial temporal sclerosis (*arrow* in a). Severe cerebellar atrophy is observed on coronal T2-weighted images (b)

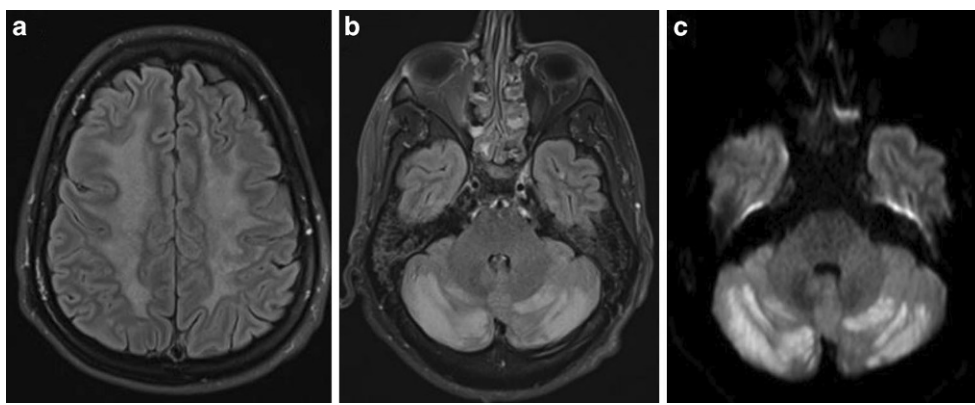
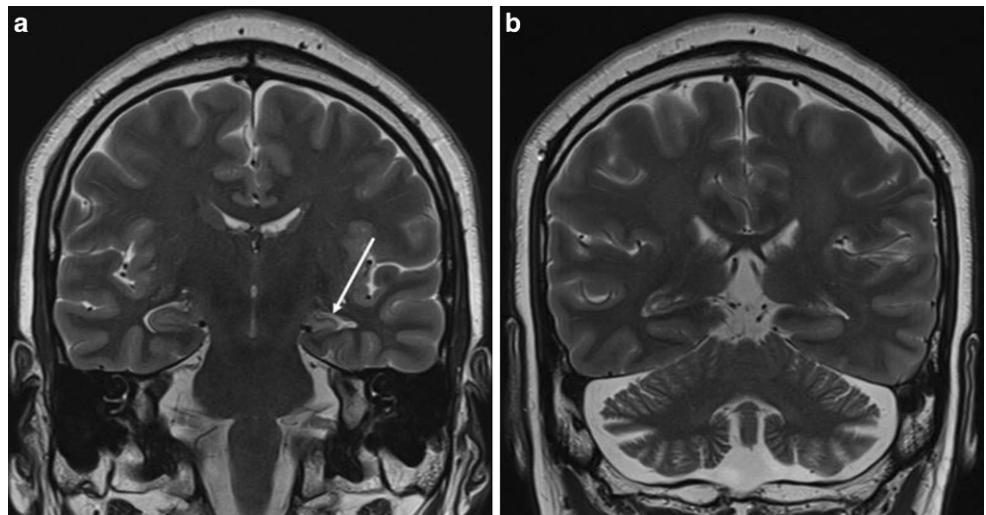


Fig. 23 Heroin-induced leukoencephalopathy (chasing the dragon) in a 40-year-old man who was comatose. Axial FLAIR images through the centrum semi-ovale (a) show extensive FLAIR-hyperintense white matter changes. FLAIR images at the level of the cerebellar hemispheres show extensive FLAIR-hyperintense changes in the cerebellar hemispheres (b) with increased signal on diffusion-weighted images (c), which in this case represented true diffusion restriction

Acquired Metabolic Disorders

The cerebellum can be involved in a wide range of acquired metabolic disorders.

In hypoxic-ischemic encephalopathy the cerebellum is typically spared in neonates, probably due to immaturity of the Purkinje cells, which gives rise to the so-called white cerebellum sign (Fig. 24; [38]). The cerebellum is less frequently spared and frequently involved in hypoxic-ischemic encephalopathy in older children and adults [36].

Posterior reversible encephalopathy syndrome (PRES) is a (usually reversible) clinical radiological syndrome characterized by neurological symptoms ranging from headache, altered mental status, seizures and vision loss, and classically associated with symmetrical parietooccipital edema. PRES has many underlying causes, including severe hypertension, drug toxicity and sepsis. Cerebellar abnormalities have been reported in up to 35% of PRES patients (Fig. 25; [39]). A central variant of PRES with predominant vaso-genic edema in the brainstem, cerebellum and basal ganglia has also been described (Fig. 26; [39]).

In patients with seizure-related imaging abnormalities, contralateral cerebellar involvement can sometimes be observed due to so-called crossed cerebellar diaschisis (Figs. 27 and 28; [40]). Cross-cerebellar diaschisis refers to a depression in cerebellar function, metabolism or perfusion due to a contralateral hemispheric cortical lesion and is a well-recognized consequence of cerebral infarction but has also been described in various other disorders that result in interruption of the crossed cortico-ponto-cerebellar white matter tracts.

Inherited Metabolic Disorders

Involvement of the cerebellum, either the cerebellar white matter, cerebellar cortex and/or dentate nuclei, can be observed in a variety of inborn errors of metabolism. Broadly speaking three possible patterns of involvement can be seen which may or may not occur together: cerebellar atrophy, abnormalities in the dentate nuclei, and abnormalities in the cerebellar white matter (non-exhaustive overview in Table 2; [41]).

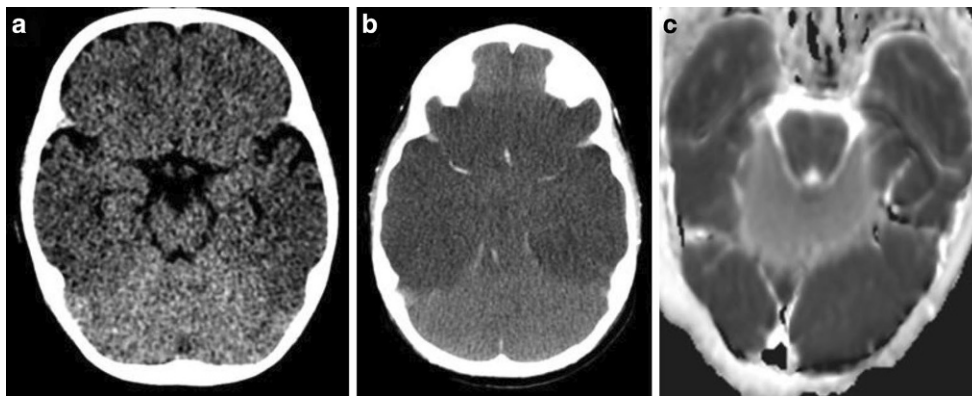
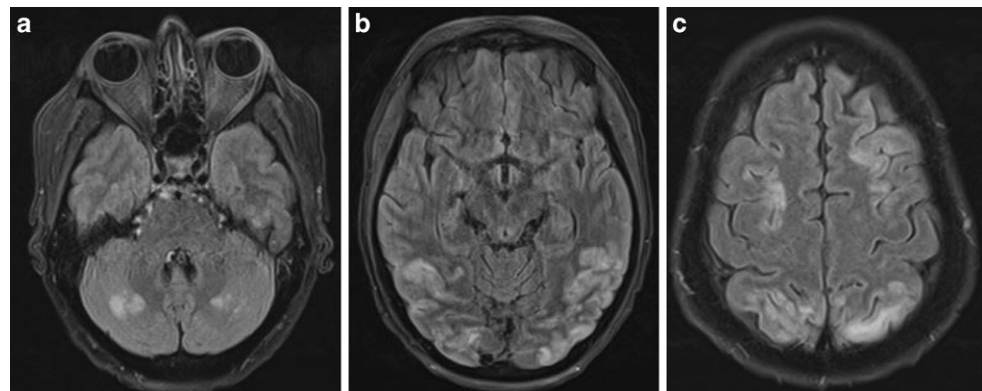


Fig. 24 Hypoxic-ischemic encephalopathy in a 3-month-old neonate (a), a 4-year old (b), and a 3-day-old infant (c). Unenhanced CT in the first two children shows hypodensity of the supratentorial brain parenchyma with obscuring of the gray-white matter differentiation. The cerebellum is not involved and appears bright in comparison to the supratentorial brain parenchyma, resulting in the so-called white cerebellum sign (a, b). MRI in patient 3 shows the equivalent of a white cerebellum sign on the ADC map, with very dark signal in the supratentorial brain parenchyma and an (in comparison) hyperintense cerebellum (c)

Fig. 25 PRES in a 43-year-old woman with acute monocytic leukemia and new onset epilepsy shortly after stem cell transplantation. Axial FLAIR images show patchy hyperintense lesions in both cerebellar hemispheres (a) as well as PRES-typical corticosubcortical FLAIR-hyperintense signal changes posteriorly in the cerebral hemispheres (b) and along the superior frontal sulci (c)



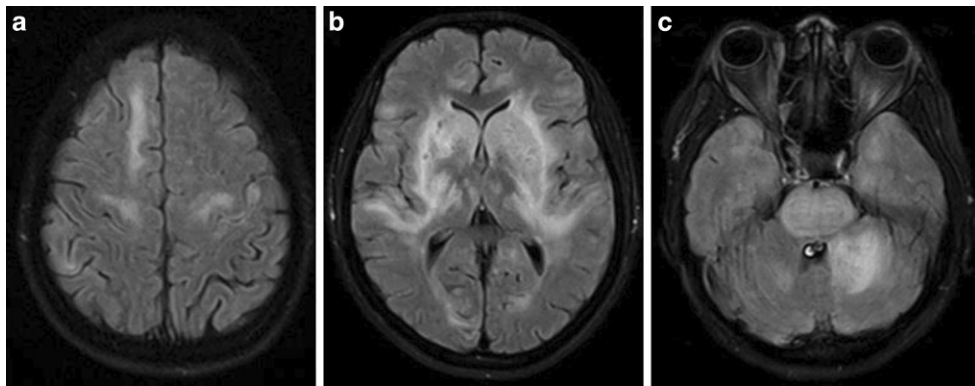


Fig. 26 Central variant of PRES (tentative diagnosis) in a 49-year-old HIV-positive woman with acute kidney failure and acute poorly controlled hypertension. Extensive edematous changes are seen on FLAIR images in the subcortical bifrontal white matter (a), in the deep grey nuclei and surrounding white matter tracts (b) and in the brainstem and cerebellar hemispheres (left more than right) (c). Treatment was focused on blood pressure control and correction of kidney function and the edematous changes regressed on follow-up imaging (images not shown)

Fig. 27 Peri-ictal imaging changes with crossed cerebellar diaschisis. Perfusion-CT images of a patient with a left-sided hemiparesis after an epileptic seizure show a right-sided holohemispheric hypoperfusion on cerebral blood flow (CBF) (a), time to peak (TTP) (b) and cerebral blood volume (CBV) maps (c) with involvement of the left cerebellar hemisphere due to crossed cerebellar diaschisis

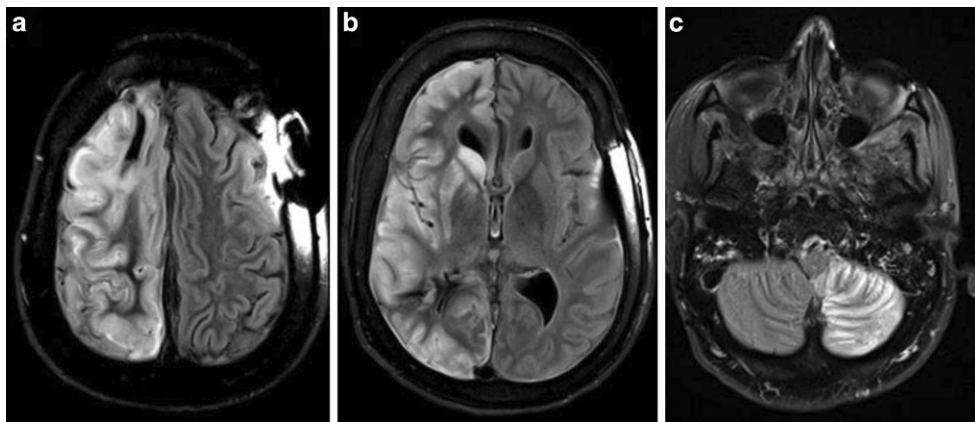
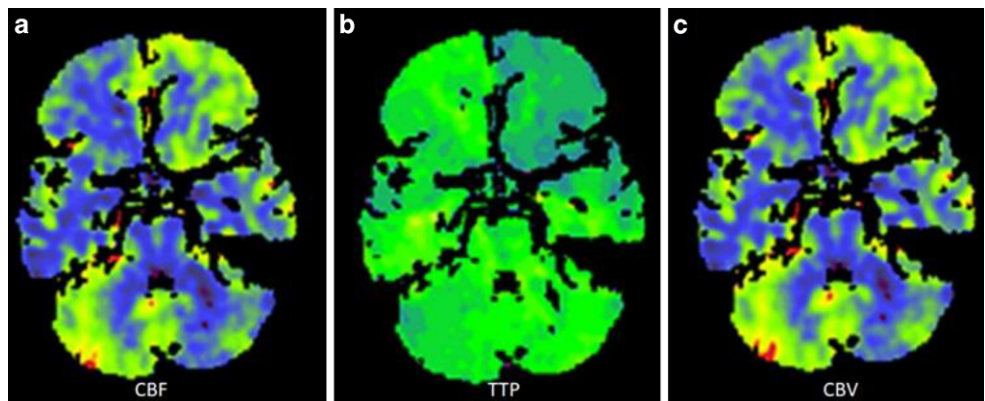


Fig. 28 Right hemispheric cortical edema with crossed cerebellar diaschisis in a 40-year-old woman found comatose at home. On axial FLAIR images there is diffuse edema of the right hemispheric cortex (a, b) and right corpus striatum (b) and edema in the contralateral cerebellar hemisphere (c). A definitive diagnosis was never found. Working diagnosis was that the patient suffered a prolonged right hemispheric status epilepticus resulting in extensive right hemispheric excitotoxic edema (evolving to laminar necrosis on follow-up imaging, images not shown) with involvement of the left cerebellum due to crossed cerebellar diaschisis

Cerebellar white matter changes or abnormalities in the dentate nuclei rarely occur in isolation, and the presence and nature of concomitant supratentorial abnormalities will often be crucial for radiological diagnosis or differential

diagnosis (Fig. 29). Cerebellar atrophy on the other hand can be an isolated or very dominant neuroradiological feature in juvenile GM2 gangliosidosis, late-infantile neuronal ceroid lipofuscinoses and Niemann-Pick disease type C and

Table 2 Cerebellar involvement in various inborn errors of metabolism

<i>Atrophy</i>	Neuronal ceroid lipofuscinosis (all types)
	Late onset GM2 gangliosidosis
	Niemann-Pick disease, type C
	Menkes disease
	Mitochondrial disorders
<i>White matter abnormalities</i>	Krabbe disease
	Pelizaeus-Merzbacher disease
	Other hypomyelinating disorders
	Maple syrup urine disease
	Alexander disease
	Canavan disease
<i>Dentate nuclei</i>	Cerebrotendinous xanthomatosis
	Infantile Refsum disease
	Krabbe disease
	L-2-Hydroxyglutaric aciduria
	Wilson disease

is also a common finding in many mitochondrial disorders (Fig. 30; [42, 43]).

Neurodegenerative Diseases

Diffuse cerebellar atrophy is a dominant feature in several sporadic and genetic neurodegenerative disorders.

Multiple system atrophy (MSA) is a sporadic neurodegenerative disease with age of onset typically between 40 and 60 years and characterized by varying degrees of cerebellar symptoms, autonomic dysfunctions, parkinsonism, and pyramidal signs. Clinically, a distinction is made between MSA-C, in which cerebellar symptoms predominate, and MSA-P in which parkinsonian signs and symptoms are the most prominent clinical findings. MSA-C is characterized by disproportionate atrophy of the cerebellum, the middle cerebellar peduncles, and the pons. In the pons, the hot cross bun sign can be present and T2-hyperintense signal abnormalities in the form of a cross representing selective degeneration of pontocerebellar tracts and median pontine raphe nuclei. In the middle cerebellar peduncles T2-hyperintense signal increase can be seen, the so-called double MCP sign, with evolution to atrophy of the middle cerebellar peduncles later in the disease course (Fig. 31). Although the hot cross bun-sign in combination with double MCP sign is very suggestive for MSA-C, the signs are not pathognomonic as they can also be seen in various other disorders, including several of the hereditary ataxia syndromes [44].

The hereditary ataxias are a very heterogeneous group of genetic disorders characterized by progressive gait ataxia, incoordination of eye movements, hand movements, and speech, and usually associated with atrophy of the cerebellum. The hereditary ataxias are generally classified ac-

cording to the mode of inheritance and the causative gene or chromosomal locus, and can be subdivided in autosomal dominant, autosomal recessive, X-linked and mitochondrial disorders. At the moment there are more than 48 known autosomal dominant types frequently termed spinocerebellar ataxia and typically presenting in adulthood, although childhood presentation occur in some forms. The most common subtypes are spinocerebellar ataxia 1, 2, 3, 6 and 7, all of which are nucleotide repeat expansion disorders [45]. Autosomal recessive ataxias usually have an onset in childhood; the most common subtypes are Friedreich ataxia, ataxia telangiectasia, and ataxia with oculomotor apraxia types 1 and 2. The neuroradiological diagnosis of hereditary ataxias can be challenging, because brain MRI often shows non-specific and overlapping imaging findings, with cerebellar atrophy as a dominant imaging abnormality [46]. Cerebellar atrophy can also be a prominent feature in hereditary spastic paraparesis syndromes, a group of genetic neurodegenerative disorders characterized by degeneration of the corticospinal tracts and posterior columns of the spinal cord (Fig. 32; [47]).

The pontocerebellar hypoplasias are a group of rare autosomal recessive neurodegenerative disorders with prenatal onset characterized by hypoplasia of the pons and cerebellum with superimposed atrophy. Up to date 11 subtypes have been identified according to their genetic basis; they show a remarkable clinical variability and differ in terms of neuroimaging findings [48]. In some cases, especially in type 2, there is more severe involvement of the cerebellar hemispheres with relative sparing of the vermis, leading to the so-called dragonfly type on coronal images (Fig. 33). Depending on the subtype, the pons may be relatively preserved or severely flattened [49]. Concomitant cerebral anomalies are frequent and include malformations of the corpus callosum in addition to atrophy especially of basal ganglia and corpus callosum.

Fahr disease/Fahr syndrome is a neurodegenerative disorder characterized by abnormal and extensive calcium depositions in the basal ganglia and dentate nuclei (Fig. 34). Subcortical white matter can also be involved. Clinically patients present with movement disorders and neuropsychiatric symptoms. There is a lot of confusion in the medical literature concerning the difference between Fahr disease and Fahr syndrome [50]. The term Fahr disease is used for genetic/familial cases in which no other explanation for the basal ganglia calcifications is found. Some authors advocate calling this disorder primary familial brain calcification. The term Fahr syndrome is reserved for cases in which a nongenetic cause for the basal ganglia calcifications is present (most frequently a parathyroid endocrinopathy) [51].

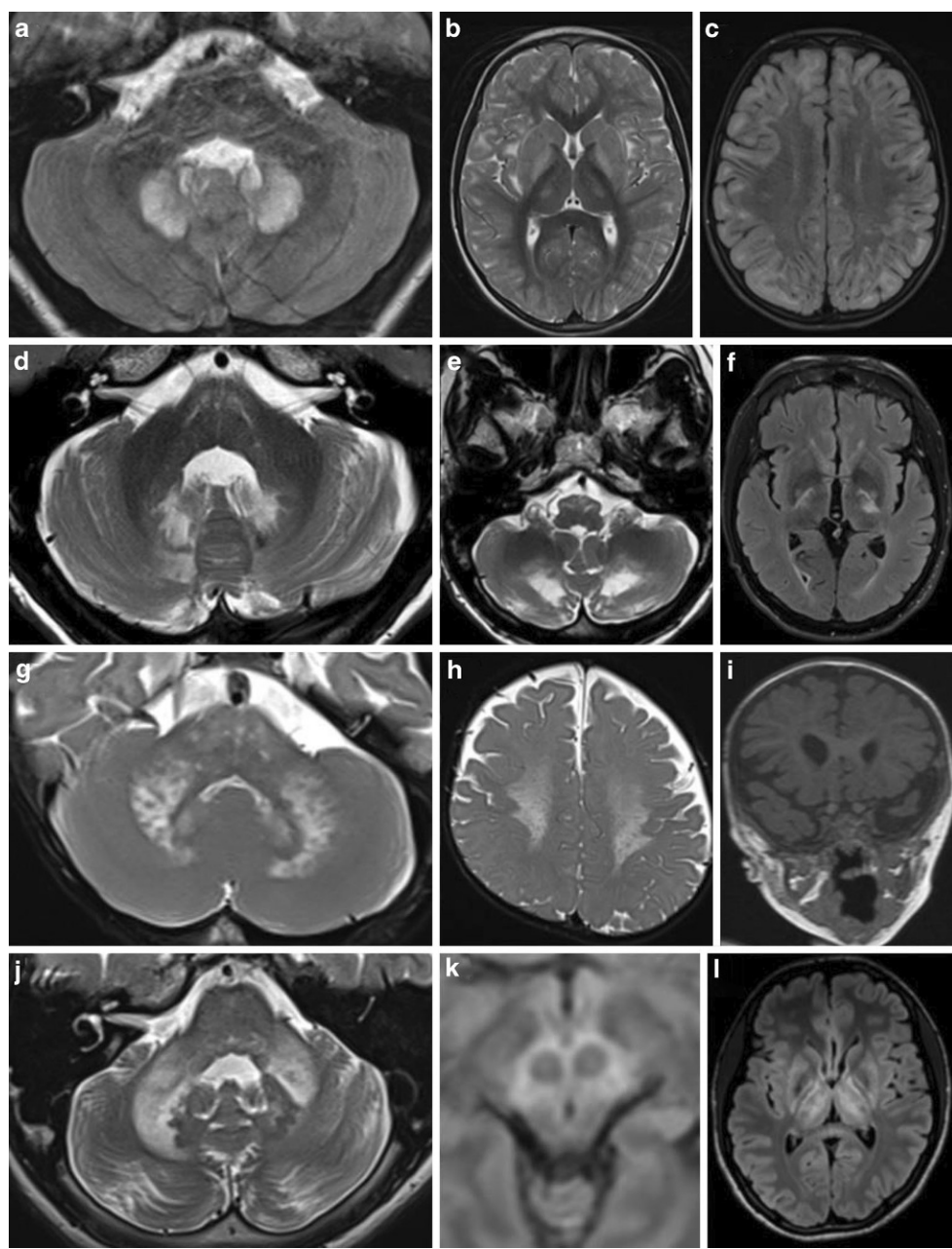


Fig. 29 Cerebellar abnormalities in various inborn errors of metabolism: L2-OH glutaric aciduria (a–c), cerebrotendinous xanthomatosis (d–f), Krabbe disease (g–i) and Wilson disease (j–l). In L2-OH glutaric acidura in a 5-year-old girl (a–c) bilateral T2 signal increase is observed in both dentate nuclei, and very extensive subcortical supratentorial white matter abnormalities (b, c). In cerebrotendinous xanthomatosis in a 44-year-old man (d–f) bilateral T2-hyperintensity is seen in both dentate nuclei (d) as well as in the deep cerebellar white matter of the corpus medullare (e). Supratentorially hyperintense T2-signal is seen in the posterior limb of the internal capsule bilaterally (f) which extends into both cerebral peduncles (images not shown). In Krabbe disease in a 7-month-old girl (g–i) T2 signal increase is seen in the hilum of both dentate nuclei, along with more extensive white matter changes with a striated appearance in both middle cerebellar peduncles and heterogeneous white matter changes in the brainstem (g). Supratentorially periventricular and deep confluent white matter changes are seen on the T2-weighted images, also with a striated appearance (h). There is significant thickening of both optic nerves on the coronal T1-weighted images (i). In Wilson disease in a 20-year-old man (j–l) extensive white matter changes are visible in both middle cerebellar peduncles on the T2-weighted images, giving rise to the so-called double MCP sign (j). There is also some T2-signal increase visible in the hilum of the dentate nuclei, on the provided image only visible on the left (j). Magnified FLAIR images over the mesencephalon show hyperintense signal centrally in the mesencephalon with sparing of the nucleus ruber, giving rise to the so-called face of the panda sign (k). FLAIR hyperintensity is also seen supratentorially in the basal ganglia and thalamus (l)

Fig. 30 Neuronal ceroid lipofuscinosis (type 7) in a 7-year-old girl with cognitive decline, epilepsy and ataxia. Axial FLAIR images show mild supratentorial atrophy (**a**) and very profound cerebellar atrophy (**b**). The difference between supratentorial and infratentorial atrophy is more striking on the axial FLAIR (**b**) and coronal T2-weighted images (**c**)

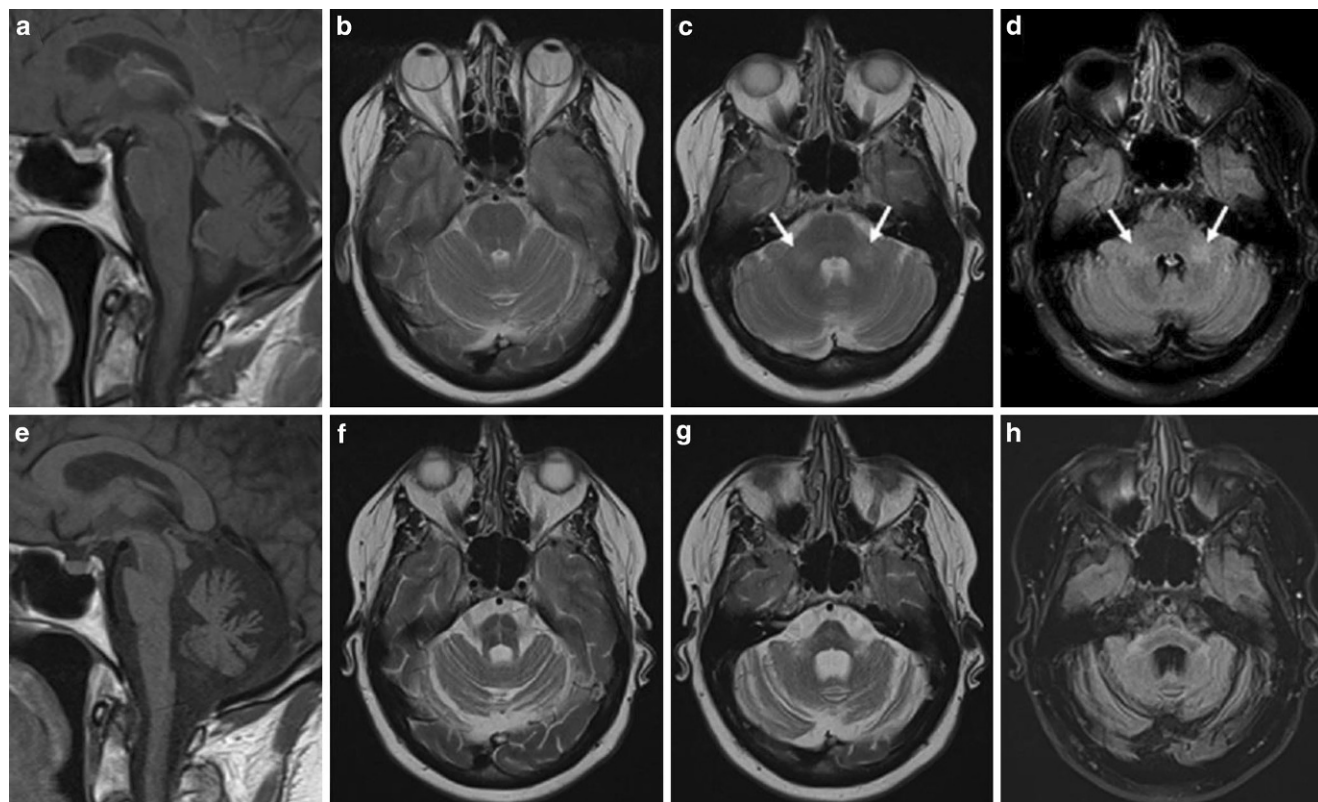
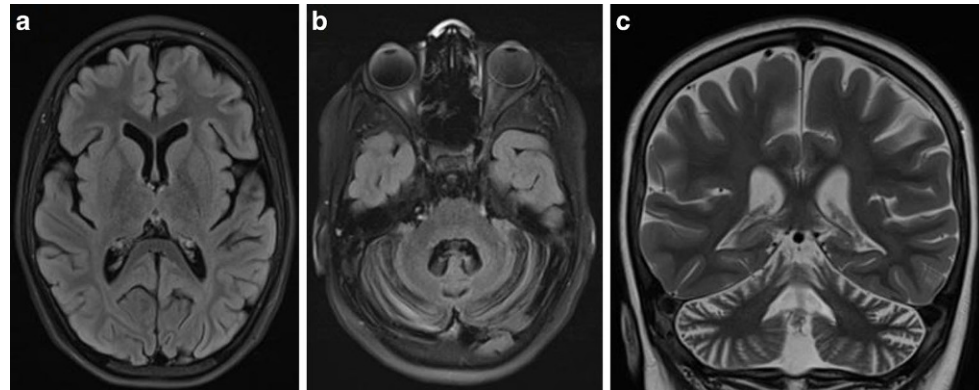


Fig. 31 MSA-C. A 59-year-old with gait disturbances (**a–d**). MRI was interpreted as normal for age. The pons and cerebellum have a normal volume on sagittal T1-weighted images (**a**) and no hot cross bun sign was observed in the pons on T2-weighted images (**b, c**). In retrospect, the beginning of a hot cross bun sign and T2-signal increase were visible in the middle cerebellar peduncles on both T2-weighted and FLAIR images (arrows in **c** and **d**). Because of progressive cerebellar symptoms repeat MRI was performed 6 years later. This time there is clear atrophy of the pons and the cerebellum (**e**), a hot cross bun sign is visible centrally in the pons (**f, g**) and there is significant atrophy of both middle cerebellar peduncles (**g, h**)

Neoplastic Disease

In adults, parenchymal metastases are the most frequent cerebellar brain tumor (Fig. 35). The posterior fossa is also a predilection site for leptomeningeal metastases, which can be detected on contrast-enhanced images as leptomeningeal enhancement in the basal cisterns and cerebellar fissures (Fig. 36). A less frequent brain tumor in adult patients but with a typical cerebellar location is hemangioblastoma. Al-

though hemangioblastoma can be entirely solid, the classical imaging appearance consists of a cystic cerebellar tumor with a contrast enhancing mural nodule (Fig. 37; [52]). Hemangioblastomas can be sporadic or occur in the context of Von Hippel-Lindau disease. In patients with Von Hippel-Lindau disease multiple hemangioblastomas may be observed, and often involve the retina and spinal cord in addition to the cerebellum. Glioblastoma, although the most frequent primary brain tumor in adult patients, is rare in the

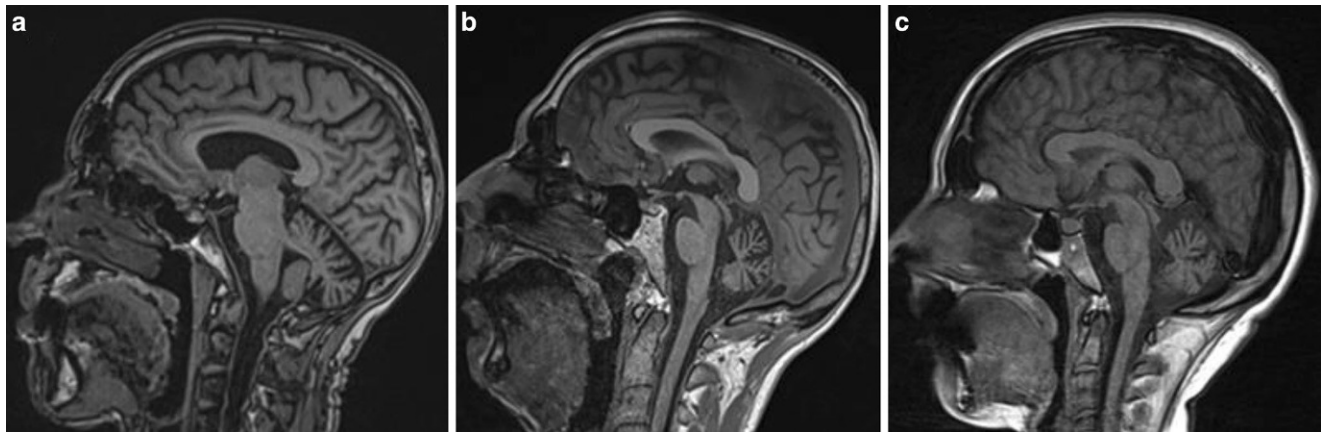


Fig. 32 Sagittal T1-weighted images in 3 patients with neurodegenerative disorders and cerebellar atrophy: spastic paraparesis 7 in a 62-year-old male (a), spastic paraparesis 78 in a 41-year-old male (b), and ataxia telangiectasia in a 21-year-old woman (c)

Fig. 33 Pontocerebellar hypoplasia type 2 in a 3-month-old girl. Sagittal T1-weighted images (a) (with degraded image quality due to motion artefacts) show a severely flattened pons and a small volume of the vermis cerebelli. On coronal T2-weighted images the dragonfly sign can be seen, caused by severe hypoplasia/atrophy of both cerebellar hemispheres and (in comparison) a relatively preserved vermis (b)

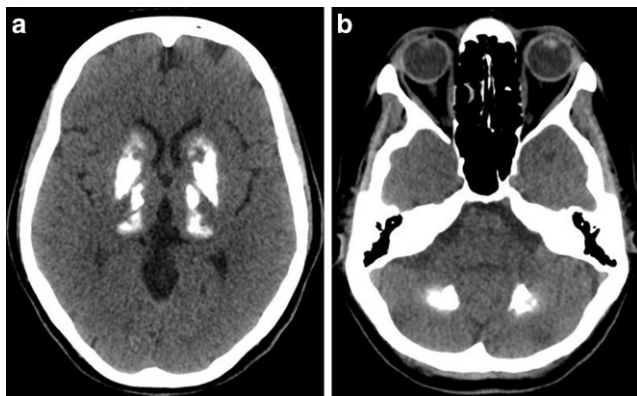
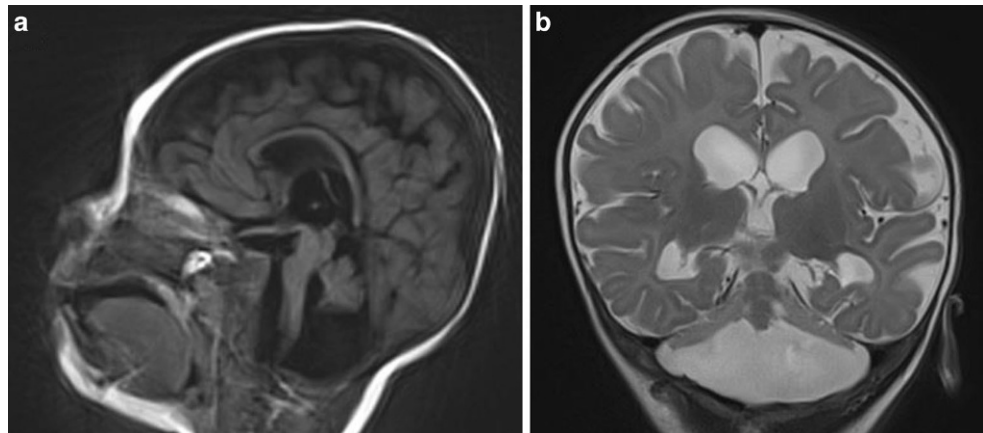


Fig. 34 Primary familial brain calcification (Fahr disease) in a 58-year-old woman with progressive extrapyramidal symptoms in the past 5 years. Unenhanced CT of the brain shows extensive coarse calcifications in the basal ganglia and thalamus (a) as well as in both dentate nuclei (b). Endocrinological and other secondary causes were excluded. Genetic screening for any of the known PFBC mutations remained negative

cerebellum, with cerebellar glioblastomas constituting only 1% of all glioblastomas [53].

In children, cerebellar metastases are rare and most tumors are primary brain tumors. The most frequent benign cerebellar tumor in children is pilocytic astrocytoma, while the most frequent malignant cerebellar tumor is medulloblastoma. Pilocytic astrocytoma often has an imaging appearance that is very similar to that of hemangioblastoma in adults, namely a cystic tumor with a contrast enhancing nodule, but may also present as a purely solid mass (Fig. 37). Medulloblastoma is a very cellular tumor which translates in diffusion restriction and decreased T2-signal intensity on MRI. Medulloblastomas show different predilection sites depending on subtype [54, 55]. Sonic hedgehog (SHH) medulloblastoma preferentially occurs in the cerebellar hemispheres and is mostly seen in infants and (young) adults (Fig. 35). The wingless (WNT) subtype is typically located in the region of the cerebellopontine angle, has the best prognosis of all medulloblastoma subtypes, and is found in children and adults. Group 3 and group 4 medulloblastomas typically occur on the midline in the region of the fourth ventricle. When a tumor looks

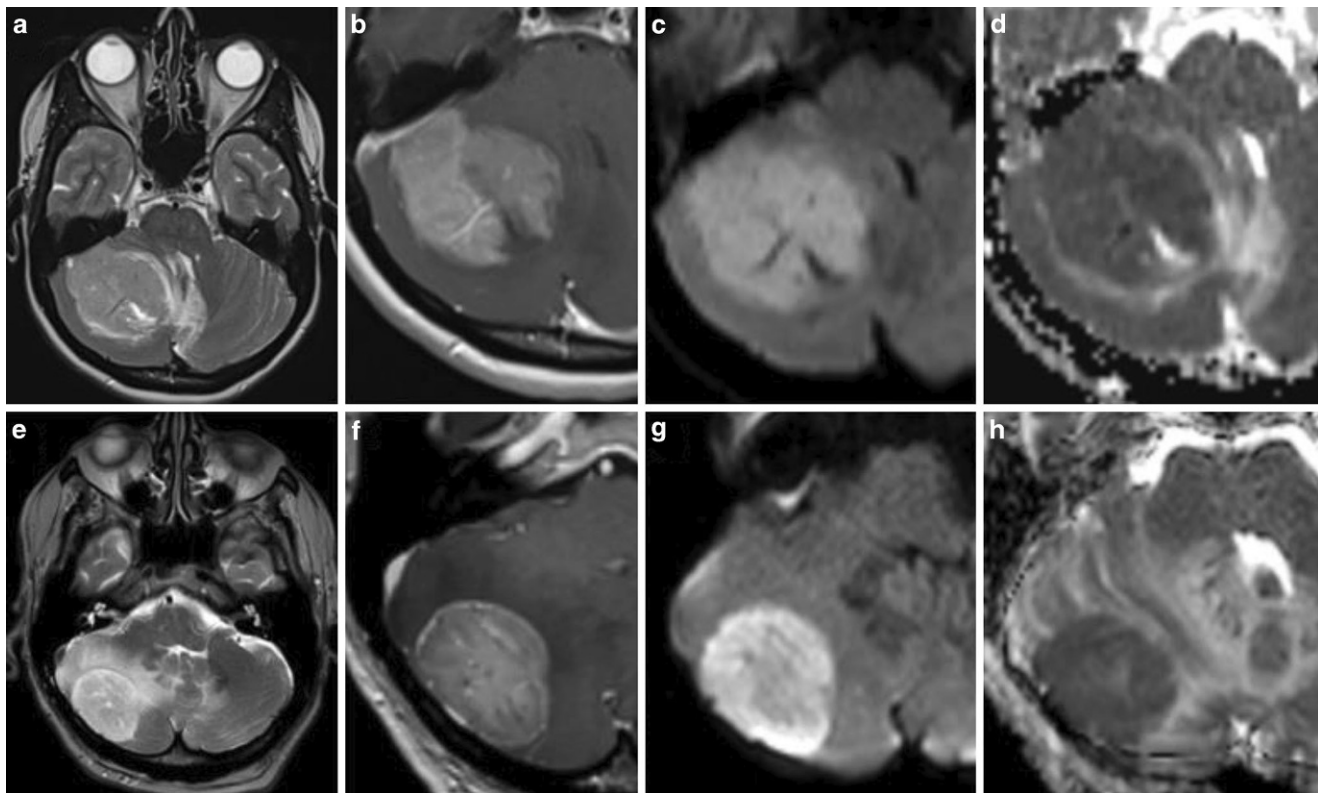


Fig. 35 Sonic hedgehog (SHH) type medulloblastoma in a young adult (32-year-old male) (a–d) and cerebellar metastases in an older patient (75-year-old male) (e–f). The tumors look very similar, composed of a large mass with perilesional edema in (a, e) with contrast enhancement (b, f) and diffusion restriction (c, d, g, h). The main differences are the demographic characteristics of both patients, with patient 1 (a–d) being a young adult with an SHH-type medulloblastoma, and patient 2 (e–h) an older patient with a cerebellar metastasis

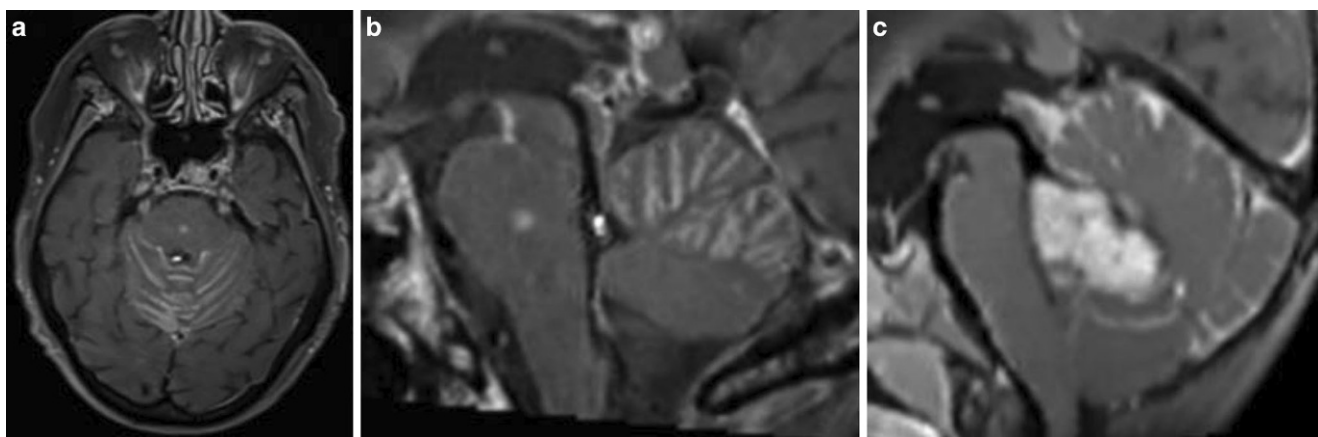


Fig. 36 Leptomeningeal metastasis (a–b) in a 62-year-old woman with metastasized breast carcinoma, and leptomeningeal seeding (c) from a primary brain tumor in a 3-year-old boy with a non-WNT/non-SHH medulloblastoma in the fourth ventricle. Axial (a) and magnified sagittal (b, c) post-contrast 3D-T1-weighted black blood images show extensive leptomeningeal enhancement in the cerebellar fissures, compatible with leptomeningeal metastasis (a–b) and seeding (c), respectively

like a medulloblastoma but is seen in a very young child (<2 years) atypical teratoid/rhabdoid tumor (AT/RT) has to be considered. Dissemination in the leptomeningeal spaces (leptomeningeal seeding) is often seen in medulloblastoma and AT/RT (as well as in other primary brain tumors that lie in direct contact with the CSF spaces) (Fig. 36).

Rosette-forming glioneuronal tumor and cerebellar dysplastic gangliocytoma (Lhermitte-Duclos disease) are rare tumors that are most frequently encountered in young adults and often have a very distinctive and easily recognizable imaging appearance. Dysplastic cerebellar gangliocytoma is a benign (WHO I) cerebellar tumor which is characterized

Fig. 37 Cerebellar pilocytic astrocytoma (a–c) in a 10-year-old boy and hemangioblastoma (d–f). Axial T2-weighted images show a large cystic lesion with an anteriorly located mural nodule (a). Contrast enhancement is seen within the mural nodule on axial (b) and coronal (c) T1-weighted images. Hemangioblastoma in a 48-year-old woman with headache and tinnitus (d–f) showing a similar tumor, consisting of a large T2-hyperintense cyst (d) with a contrast-enhancing nodule (e, f)

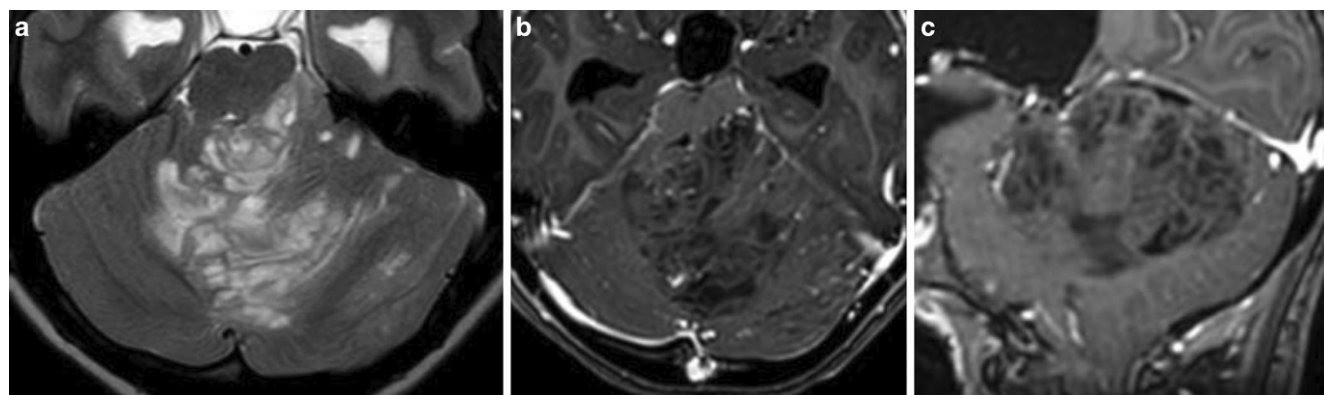
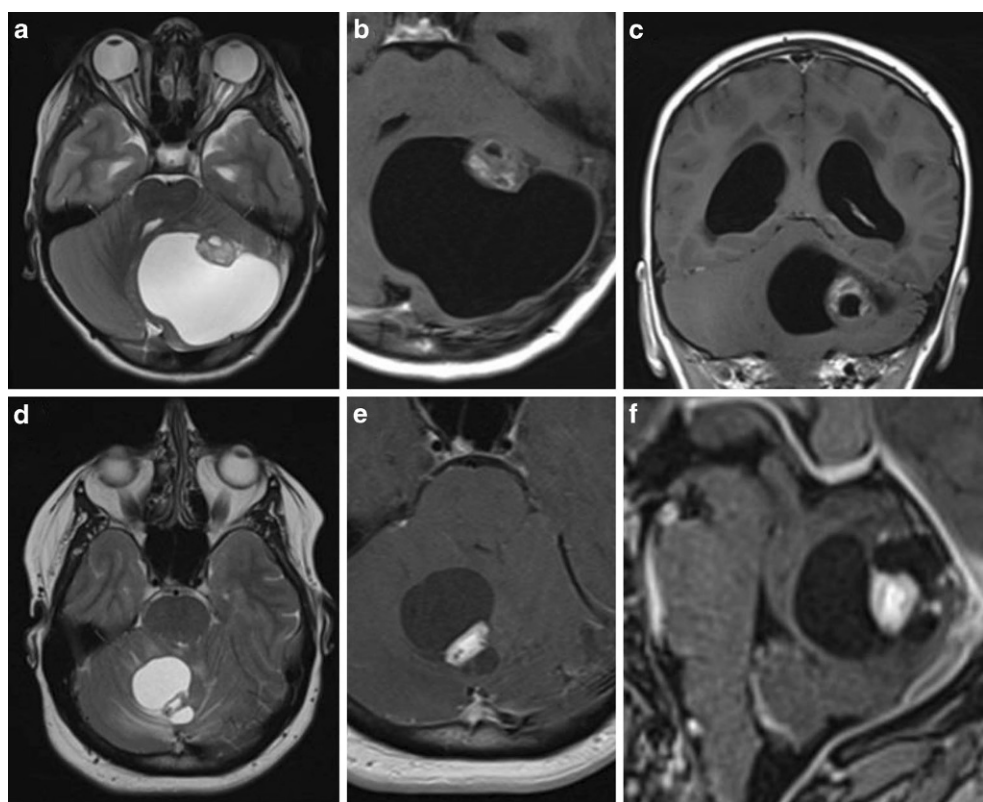


Fig. 38 Dysplastic cerebellar gangliocytoma (Lhermitte-Duclos disease) in a 24-year-old woman presenting with headache. Axial T2-weighted images (a) and post-contrast axial (b) and sagittal T1-weighted images (c) show a space-occupying intra-axial tumor centered in the left cerebellar hemisphere with contralateral extension, left transinscircular upward herniation and obstructive hydrocephalus. The tumor shows a striated or corduroy appearance on both T2-weighted and T1-weighted images without enhancement

by thickening and T2-signal increase of the cerebellar folia, resulting in a striated (corduroy) appearance typical for the tumor (Fig. 38). The tumor is associated with Cowden syndrome. Rosette-forming glioneuronal tumors are rare benign (WHO I) midline tumors that are usually found in the region of the 4th ventricle and often contain cystic components. The tumor shows no or little heterogeneous contrast enhancement (Fig. 39).

Congenital Malformations

The spectrum of congenital malformations in the posterior fossa is broad and complex. Cerebellar malformations can occur in isolation but are often part of a broader cystic posterior fossa or hindbrain malformation, which may be divided into two main groups: large extracerebellar and small intracerebellar cystic malformations [56]. An adequate discussion of this topic would require a review on its own and is beyond the scope of this article [49].

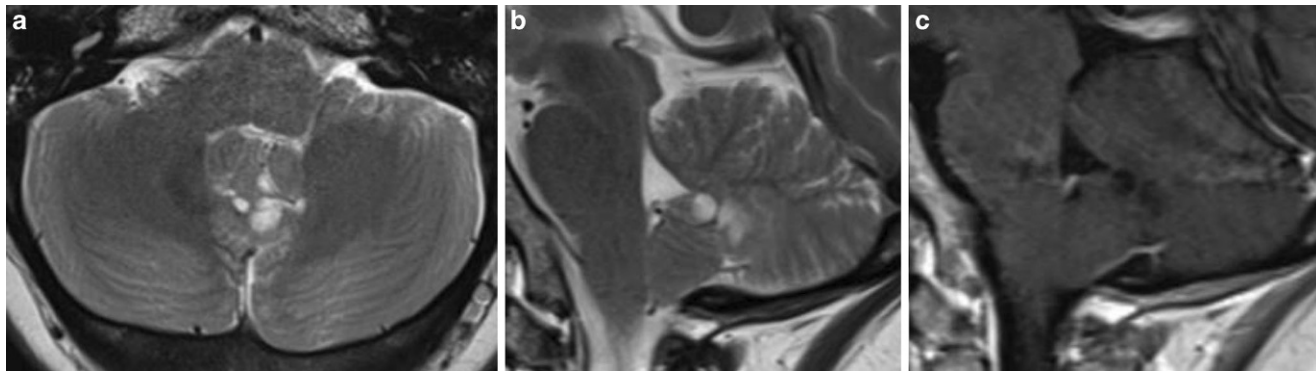


Fig. 39 Rosette-forming glioneuronal tumor in a 31-year-old woman with acute unstable gait and word finding difficulties. Axial (**a**) and sagittal (**b**) T2-weighted images show a multicystic lesion in the vermis cerebelli, immediately posterior of the fastigium of the fourth ventricle. No contrast enhancement is seen on the T1-weighted images with gadolinium (**c**)

Conclusion

The cerebellum is a functionally important part of the brain and plays an important role in motor movement regulation and balance control, as well as in higher order cognitive functions. The cerebellum can be involved in a wide range of pathological processes. Knowledge and familiarity with the characteristic imaging manifestations of these disorders is important in reaching a sound (differential) diagnosis.

Acknowledgements The authors would like to thank Dr. Johannes Devos, Department of Radiology, UZ Gasthuisberg Leuven, Belgium and Dr. Sofie van Cauter Department of Radiologie, Ziekenhuis Oost-Limburg (ZOL) Genk, Belgium for providing cases.

Conflict of interest S. Dekeyzer, S. Vanden Bossche and L. De Cocker declare that they have no competing interests.

References

- Roostaei T, Nazeri A, Sahraian MA, et al. The human cerebellum: a review of physiologic neuroanatomy. *Neurol Clin*. 2014;32:859–69. <https://doi.org/10.1016/j.ncl.2014.07.013>.
- Schmahmann JD, Doyon J, McDonald D, et al. Three-dimensional MRI atlas of the human cerebellum in proportional stereotaxic space. *Neuroimage*. 1999;10:233–60. <https://doi.org/10.1006/nimg.1999.0459>.
- Voogd J, Nieuwenhuys R. The human central nervous system. Springer; 1988. pp. 807–34.
- Courchesne E, Press GA, Murakami J, et al. The cerebellum in sagittal plane—anatomic-MR correlation: 1. The vermis. *AJR Am J Roentgenol*. 1989;153:829–35. <https://doi.org/10.2214/ajr.153.4.829>.
- Press GA, Murakami J, Courchesne E, et al. The cerebellum in sagittal plane—anatomic-MR correlation: 2. The cerebellar hemispheres. *AJR Am J Roentgenol*. 1989;153:837–46. <https://doi.org/10.2214/ajr.153.4.837>.
- Press GA, Murakami JW, Courchesne E, et al. The cerebellum: 3. Anatomic-MR correlation in the coronal plane. *AJR Am J Roentgenol*. 1990;154:593–602. <https://doi.org/10.2214/ajr.154.3.2106226>.
- Sereno MI, Diedrichsen J, Tachroud M, et al. The human cerebellum has almost 80 % of the surface area of the neocortex. *Proc Natl Acad Sci USA*. 2020;117:19538–43. <https://doi.org/10.1073/pnas.2002896117>.
- De Cocker LJ, Lövblad KO, Hendrikse J. MRI of cerebellar infarction. *Eur Neurol*. 2017;77:137–46. <https://doi.org/10.1159/000455229>.
- Hartkamp NS, De Cocker LJ, Helle M, et al. In vivo visualization of the PICA perfusion territory with super-selective pseudo-continuous arterial spin labeling MRI. *Neuroimage*. 2013;83:58–65. <https://doi.org/10.1016/j.neuroimage.2013.06.070>.
- Klein AP, Ulmer JL, Quinet SA, et al. Nonmotor functions of the cerebellum: an introduction. *AJNR Am J Neuroradiol*. 2016;37:1005–9.
- Acosta-Cabronero J, Betts MJ, Cardenas-Blanco A, et al. In vivo MRI mapping of brain iron deposition across the adult lifespan. *J Neurosci*. 2016;36:364–74. <https://doi.org/10.1523/JNEUROSCI.1907-15.2016>.
- Mallio CA, Quattrocchi CC, Rovira À, et al. Gadolinium deposition safety: seeking the patient's perspective. *AJNR Am J Neuroradiol*. 2020;41:944–6. <https://doi.org/10.3174/ajnr.A6586>.
- Wright J, Huang C, Strbian D, et al. Diagnosis and management of acute cerebellar infarction. *Stroke*. 2014;45:e56–e8. <https://doi.org/10.1161/STROKEAHA.114.004474>.
- De Cocker LJ, Geerlings MI, Hartkamp NS, SMART study group, et al. Cerebellar infarct patterns: the SMART-medea study. *Neuroimage Clin*. 2015;8:314–21. <https://doi.org/10.1016/j.nicl.2015.02.001>.
- Wright JN, Shaw DWW, Ishak G, et al. Cerebellar watershed injury in children. *Ajnr Am J Neuroradiol*. 2020;41:923–8. <https://doi.org/10.3174/ajnr.A6532>.
- De Cocker LJ, Hendrikse J. Depth-of-fissure cerebellar infarcts in adults. *Ajnr Am J Neuroradiol*. 2020;41:E60. <https://doi.org/10.3174/ajnr.A6626>.
- De Cocker LJ, Kloppenborg RP, van der Graaf Y, et al. Cerebellar cortical infarct cavities: correlation with risk factors and MRI markers of cerebrovascular disease. *Stroke*. 2015;46:3154–60. <https://doi.org/10.1161/STROKEAHA.115.010093>.
- De Cocker LJ, Compter A, Kappelle LJ, et al. Cerebellar cortical infarct cavities and vertebral artery disease. *Neuroradiology*. 2016;58:853–7. <https://doi.org/10.1007/s00234-016-1707-9>.
- Ter Schiphorst A, Tatu L, Thijs V, et al. Small obliquely oriented cortical cerebellar infarctions are associated with cardioembolic stroke. *BMC Neurol*. 2019;19:100. <https://doi.org/10.1186/s12883-019-1328-0>.

20. Datar S, Rabenstein AA. Cerebellar hemorrhage. *Neurol Clin.* 2014;32:993–1007. <https://doi.org/10.1016/j.ncl.2014.07.006>.
21. Pasi M, Marini S, Morotti A, et al. Cerebellar hematoma location: implications for the underlying microangiopathy. *Stroke.* 2018;49:207–10. <https://doi.org/10.1161/STROKEAHA.117.019286>.
22. Negro A, Somma F, Piscitelli V, et al. Intracranial hemorrhage from dural arteriovenous fistulas: what can we find with CT angiography? *Tomography.* 2021;7:804–14. <https://doi.org/10.3390/tomography7040068>.
23. Amini A, Osborn AG, McCall TD, et al. Remote cerebellar hemorrhage. *AJNR Am J Neuroradiol.* 2006;27:387–90.
24. Rossi A, Martinetti C, Morana G, et al. Neuroimaging of infectious and inflammatory diseases of the pediatric cerebellum and brainstem. *Neuroimaging Clin N Am.* 2016;26:471–87. <https://doi.org/10.1016/j.nic.2016.03.011>.
25. Pruitt AA. Infections of the cerebellum. *Neurol Clin.* 2014;32: 1117–31. <https://doi.org/10.1016/j.ncl.2014.07.009>.
26. Kayaaslan BU, Akinci E, Bilen S, et al. Listerial rhombencephalitis in an immunocompetent young adult. *Int J Infect Dis.* 2009;13:e65–7. <https://doi.org/10.1016/j.ijid.2008.06.026>.
27. Loehr PA, Zieger L, Simon OJ. Update on paraneoplastic cerebellar degeneration. *Brain Sci.* 2021;11:1414. <https://doi.org/10.3390/brainsci11111414>.
28. Napolitano M, Ranieri A, Alfieri G, et al. Paraneoplastic cerebellar degeneration associated with anti-Yo antibodies appearing as a leptomeningeal cerebellar carcinomatosis at MRI: a case report. *SN Compr Clin Med.* 2021;3:2329–31. <https://doi.org/10.1007/s42399-021-01002-2>.
29. Fredriksen JR, Carr CM, Koeller KK, et al. MRI findings in glutamic acid decarboxylase associated autoimmune epilepsy. *Neuroradiology.* 2018;60:239–45.
30. Dudesek A, Rimmehle F, Tesar S, et al. CLIPPERS: chronic lymphocytic inflammation with pontine perivascular enhancement responsive to steroids. Review of an increasingly recognized entity within the spectrum of inflammatory central nervous system disorders. *Clin Exp Immunol.* 2014;175:385–96. <https://doi.org/10.1111/cei.12204>.
31. Obeidat AZ, Block AN, Hooshmand SI. “Peppering the pons”: CLIPPERS or myelin oligodendrocyte glycoprotein associated disease? *Mult Scler Relat Disord.* 2021;51:102874. <https://doi.org/10.1016/j.msard.2021.102874>.
32. Bag AK, Curé JK, Chapman PR, et al. JC virus infection of the brain. *AJNR Am J Neuroradiol.* 2010;31:1564–76. <https://doi.org/10.3174/ajnr.A2035>.
33. Adra N, Goodheart AE, Rapalino O, et al. MRI shrimp sign in cerebellar progressive multifocal leukoencephalopathy: description and validation of a novel observation. *AJNR Am J Neuroradiol.* 2021;42:1073–9. <https://doi.org/10.3174/ajnr.A7145>.
34. Wijburg MT, van Oosten BW, Murk JL, et al. Heterogeneous imaging characteristics of JC virus granule cell neuronopathy (GCN): a case series and review of the literature. *J Neurol.* 2015;262:65–73. <https://doi.org/10.1007/s00415-014-7530-5>.
35. Mitoma H, Manto M, Shaikh AG. Mechanisms of ethanol-induced cerebellar ataxia: underpinnings of neuronal death in the cerebellum. *Int J Environ Res Public Health.* 2021;18:8678. <https://doi.org/10.3390/ijerph18168678>.
36. de Oliveira AM, Paulino MV, Vieira APF, et al. Imaging patterns of toxic and metabolic brain disorders. *Radiographics.* 2019;39:1672–95. <https://doi.org/10.1148/rg.2019190016>.
37. Alqahtani H, Shirah B, Alqahtani AJ, et al. Irreversible cerebellar atrophy as a complication of short-term phenytoin exposure: clinical improvement following discontinuation of the culprit. *J Epilepsy Res.* 2020;10:96–9. <https://doi.org/10.14581/jer.20016>.
38. Huang BY, Castillo M. Hypoxic-ischemic brain injury: imaging findings from birth to adulthood. *Radiographics.* 2008;28:417–39.
39. McKinney AM, Short J, Truwit CL, et al. Posterior reversible encephalopathy syndrome: incidence of atypical regions of involvement and imaging findings. *AJR Am J Roentgenol.* 2007;189:904–12. <https://doi.org/10.2214/AJR.07.2024>.
40. Belfkih R, Khayat OG, Berkaoui A, et al. Crossed cerebellar diaschisis in the setting of a convulsive status epilepticus: a rare clinical and radiological entity. *Radiol Case Rep.* 2021;16:2913–5. <https://doi.org/10.1016/j.radcr.2021.06.092>.
41. Steinlin M, Blaser S, Boltshauser E. Cerebellar involvement in metabolic disorders: a pattern-recognition approach. *Neuroradiology.* 1998;40:347–54. <https://doi.org/10.1007/s002340050597>.
42. Poretti A, Wolf NI, Boltshauser E. Differential diagnosis of cerebellar atrophy in childhood: an update. *Neuropediatrics.* 2015;46:359–70. <https://doi.org/10.1055/s-0035-1564620>.
43. Finsterer J, Zarrouk-Mahjoub S. Cerebellar atrophy is common among mitochondrial disorders. *Metab Brain Dis.* 2018;33:987–8. <https://doi.org/10.1007/s11011-018-0238-y>.
44. Okamoto K, Tokiguchi S, Furusawa T, et al. MR features of diseases involving bilateral middle cerebellar peduncles. *AJNR Am J Neuroradiol.* 2003;24:1946–54.
45. Kurokawa R, Kurokawa M, Mitsutake A, et al. Clinical and neuroimaging review of triplet repeat diseases. *Jpn J Radiol.* 2003;41:115–30. <https://doi.org/10.1007/s11604-022-01343-5>.
46. Cocozza S, Pontillo G, De Michele G, et al. Conventional MRI findings in hereditary degenerative ataxias: a pictorial review. *Neuroradiology.* 2021;63:983–99. <https://doi.org/10.1007/s00234-021-02682-2>.
47. Shribman S, Reid E, Crosby AH, et al. Hereditary spastic paraparesis: from diagnosis to emerging therapeutic approaches. *Lancet Neurol.* 2019;18:1136–46. [https://doi.org/10.1016/S1474-4422\(19\)30235-2](https://doi.org/10.1016/S1474-4422(19)30235-2).
48. Scola E, Ganau M, Robinson R, et al. Neuroradiological findings in three cases of pontocerebellar hypoplasia type 9 due to AMPD2 mutation: typical MRI appearances and pearls for differential diagnosis. *Quant Imaging Med Surg.* 2019;9:1966–72. <https://doi.org/10.21037/qims.2019.08.12>.
49. Bosemani T, Orman G, Boltshauser E, et al. Congenital abnormalities of the posterior fossa. *Radiographics.* 2015;35:200–20. <https://doi.org/10.1148/rg.351140038>.
50. Primary familial brain calcification.. <https://www.ncbi.nlm.nih.gov/books/NBK1421/>. Accessed 11 Apr 2014.
51. Perugula ML, Lippmann S. Fahr’s disease or Fahr’s syndrome? *Innov Clin Neurosci.* 2016;13:45–6.
52. Kim EH, Moon JH, Kang SG, et al. Diagnostic challenges of posterior fossa hemangioblastomas: refining current radiological classification scheme. *Sci Rep.* 2020;10:6267. <https://doi.org/10.1038/s41598-020-63207-0>.
53. Hur H, Jung S, Jung TY, et al. Cerebellar glioblastoma multiforme in an adult. *J Korean Neurosurg Soc.* 2008;43:194–7. <https://doi.org/10.3340/jkns.2008.43.4.194>.
54. Perreault S, Ramaswamy V, Achrol AS, et al. MRI surrogates for molecular subgroups of medulloblastoma. *AJNR Am J Neuroradiol.* 2014;35:1263–9. <https://doi.org/10.3174/ajnr.A3990>.
55. Keil VC, Warmuth-Metz M, Reh C, et al. Imaging biomarkers for adult medulloblastomas: genetic entities may be identified by their MR imaging radiophenotype. *AJNR Am J Neuroradiol.* 2017;38:1892–8. <https://doi.org/10.3174/ajnr.A5313>.
56. Poretti A, Bolemani T. Cystic malformations within the posterior fossa. *Curr Radiol Rep.* 2016;4:17. <https://doi.org/10.1007/s40134-016-0147-y>.

Springer Nature or its licensor (e.g. a society or other partner) holds exclusive rights to this article under a publishing agreement with the author(s) or other rightsholder(s); author self-archiving of the accepted manuscript version of this article is solely governed by the terms of such publishing agreement and applicable law.

Terms and Conditions

Springer Nature journal content, brought to you courtesy of Springer Nature Customer Service Center GmbH (“Springer Nature”). Springer Nature supports a reasonable amount of sharing of research papers by authors, subscribers and authorised users (“Users”), for small-scale personal, non-commercial use provided that all copyright, trade and service marks and other proprietary notices are maintained. By accessing, sharing, receiving or otherwise using the Springer Nature journal content you agree to these terms of use (“Terms”). For these purposes, Springer Nature considers academic use (by researchers and students) to be non-commercial.

These Terms are supplementary and will apply in addition to any applicable website terms and conditions, a relevant site licence or a personal subscription. These Terms will prevail over any conflict or ambiguity with regards to the relevant terms, a site licence or a personal subscription (to the extent of the conflict or ambiguity only). For Creative Commons-licensed articles, the terms of the Creative Commons license used will apply.

We collect and use personal data to provide access to the Springer Nature journal content. We may also use these personal data internally within ResearchGate and Springer Nature and as agreed share it, in an anonymised way, for purposes of tracking, analysis and reporting. We will not otherwise disclose your personal data outside the ResearchGate or the Springer Nature group of companies unless we have your permission as detailed in the Privacy Policy.

While Users may use the Springer Nature journal content for small scale, personal non-commercial use, it is important to note that Users may not:

1. use such content for the purpose of providing other users with access on a regular or large scale basis or as a means to circumvent access control;
2. use such content where to do so would be considered a criminal or statutory offence in any jurisdiction, or gives rise to civil liability, or is otherwise unlawful;
3. falsely or misleadingly imply or suggest endorsement, approval , sponsorship, or association unless explicitly agreed to by Springer Nature in writing;
4. use bots or other automated methods to access the content or redirect messages
5. override any security feature or exclusionary protocol; or
6. share the content in order to create substitute for Springer Nature products or services or a systematic database of Springer Nature journal content.

In line with the restriction against commercial use, Springer Nature does not permit the creation of a product or service that creates revenue, royalties, rent or income from our content or its inclusion as part of a paid for service or for other commercial gain. Springer Nature journal content cannot be used for inter-library loans and librarians may not upload Springer Nature journal content on a large scale into their, or any other, institutional repository.

These terms of use are reviewed regularly and may be amended at any time. Springer Nature is not obligated to publish any information or content on this website and may remove it or features or functionality at our sole discretion, at any time with or without notice. Springer Nature may revoke this licence to you at any time and remove access to any copies of the Springer Nature journal content which have been saved.

To the fullest extent permitted by law, Springer Nature makes no warranties, representations or guarantees to Users, either express or implied with respect to the Springer nature journal content and all parties disclaim and waive any implied warranties or warranties imposed by law, including merchantability or fitness for any particular purpose.

Please note that these rights do not automatically extend to content, data or other material published by Springer Nature that may be licensed from third parties.

If you would like to use or distribute our Springer Nature journal content to a wider audience or on a regular basis or in any other manner not expressly permitted by these Terms, please contact Springer Nature at

onlineservice@springernature.com